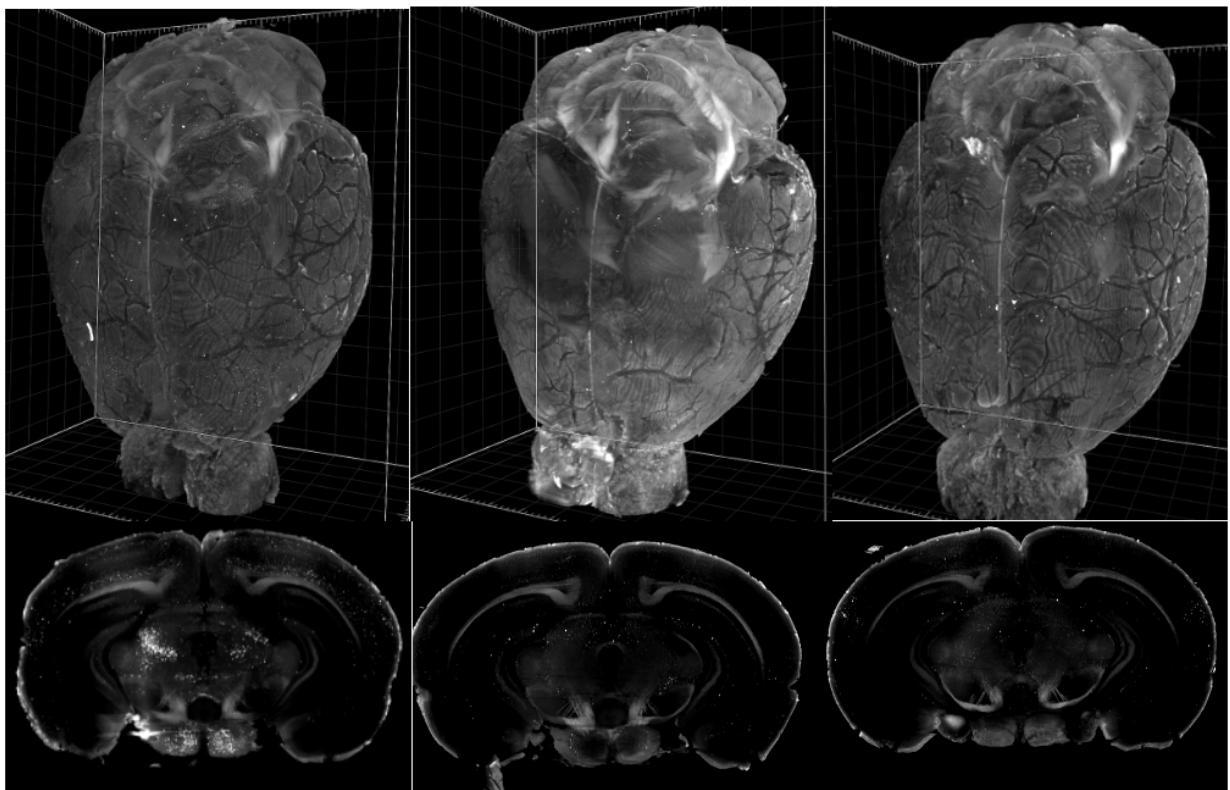


Whole-brain imaging for comparing the supraspinal effects of mPD5 to morphine in a mouse model of neuropathic pain

Master thesis
Laura Reinholdt Knudsen
Aalborg University
Translational medicine, 10th Semester



Title page

Title of project

Whole-brain imaging for comparing the supraspinal effects of mPD5 to morphine in a mouse model of neuropathic pain

Type of Project

Experimental study

Name and student number

Laura Reinholdt Knudsen, 20183595

Education

Medicine with Industrial Specialisation, Translational medicine

Group number

9015

Class of

2018-2024 (10th Semester)

Internal Supervisor

Kristian Kjær Pedersen & Maj Schneider

External Supervisor

Kenneth L. Madsen

Laboratory technicians

Sara Jager & Kathrine Jensen

Institution of education

Aalborg University

External collaboration

Copenhagen University, Panum

Submission date

31.05.2024

Keystrokes

12887

Abstract

Introduction:

Neuropathic pain, a global health concern affecting 20% of the adult population, has proven difficult to treat. The current treatment options have demonstrated poor efficacy and outcomes. Additionally, 21-29% of patients prescribed opioids misuse them, with 8-10% of patients developing an opioid addiction. Despite the low efficacy of opioids, neuropathic pain patients continue to be prescribed these medications. This underscores the need for better pain management options for neuropathic pain patients. One of the etiologies of neuropathic pain is maladaptive changes in the synapses of the dorsal horn in the medulla spinalis. Protein interacting with C kinase 1 (PICK1) is a scaffold protein involved in the maladaptive changes observed in neuropathic pain conditions. Myr-NPEG₄-(HWLKV)₂, commonly referred to as mPD5, is a bivalent peptide inhibitor of the scaffold protein PICK1. Its function is to block the effects of PICK1 and mediate pain relief in chronic pain conditions.

Aim:

The aim of this study is to assess whether the spared nerve injury (SNI) mouse model, results in supraspinal c-Fos changes compared to naive mice. Moreover, the aim of this study is to compare the supra spinal effects of mPD5 to morphine in an SNI model, with focus on selected brain areas processing nociceptive information.

Method:

Tissue clearing and immunolabeling with c-Fos as a proxy for neuronal activity was the chosen method for this study, as it facilitates whole-brain imaging and enables three-dimensional visualization of deep structures in the brain. After mice brains (n=74) were imaged with a light sheet microscope, the images were stitched, aligned to a mouse atlas, and analyzed using a customized Python script. To investigate the differences in whole-brain c-Fos positive cells between the treatments and phosphate buffered saline (PBS) groups, a non-parametric Kruskal-Wallis test was performed. Next, a region-wise comparison analysis (Mann-Whitney U test) was conducted and presented using volcano plots, to examine the differences in brain regions' c-Fos positive cells between the treatments and PBS groups.

Results:

The Mann-Whitney U test showed no significant difference in whole-brain total c-Fos positive cell counts between the non-treated naive and SNI mice, but on a region wise level a few differences were observed. The Kruskal-Wallis test showed a significant ($p < 0.05$) difference between morphine and mPD5 for both naive and SNI mice (SNI $p = 0.0014$ and naive $p = 0.023$) as well as a significant ($p < 0.05$) difference between morphine and PBS in both naive and SNI mice (SNI $p = 0.007$ and naive $p = 0.0002$). The volcano plots showed that mPD5 induced activity in brain regions processing nociceptive information.

Conclusion:

This study demonstrated the activity-inducing effects of mPD5 in brain areas processing nociceptive information. Moreover, it showed that mPD5 has far less activity-inducing effect on the brain compared to morphine and does not appear to present the same addictive properties as morphine. This advocates that mPD5 represents a promising drug candidate for further preclinical testing before proceeding to clinical trials and treatment of neuropathic pain.

Resumé

Indledning:

Neuropatisk smerte, en global sundhedsmæssig bekymring, der påvirker 20% af den voksne befolkning, har vist sig at være vanskelig at behandle. De nuværende behandlingsmuligheder har vist ringe effekt og resultater. Derudover misbruger 21-29% af patienter, der får ordineret opioider disse, hvoraf 8-10% udvikler en opioidafhængighed. På trods af den lave effektivitet af opioider fortsætter neuropatiske smertepatienter med at få ordineret disse medikamenter. Dette understreger behovet for bedre smertehåndteringsmuligheder for neuropatiske smertepatienter. En af årsagerne til neuropatisk smerte er maladaptive ændringer i synapserne i dorsalhornet i medulla spinalis. PICK1 er et scaffold-protein involveret i de maladaptive ændringer, der observeres i neuropatiske smertetilstande. mPD5 er en bivalent peptidinhibitor af PICK1. Dens funktion er at blokere virkningerne af PICK1 og mediere smertelindring ved blandt andet neuropatiske smertetilstande.

Formål:

Formålet med denne undersøgelse er at vurdere, om SNI-modellen hos mus resulterer i supraspinale c-Fos-ændringer sammenlignet med naive mus. Desuden er formålet med denne undersøgelse at sammenligne de supraspinale effekter af mPD5 med morfin i en SNI-model med fokus på udvalgte hjerneområder, der behandler nociceptive informationer.

Metode:

Vævs-clearing og farvning med c-Fos som en proxy for neuronal aktivitet var den valgte metode til denne undersøgelse, da det letter helhjerneafbildning og muliggør 3D-visualisering af dybe strukturer i hjernen. Efter at mussehjernerne (n=74) blev afbildet med et lightsheet-mikroskop, blev billederne sammenstykket, justeret til et museatlas og analyseret ved hjælp af et tilpasset Python-script. For at undersøge forskellene i hele hjernens c-Fos positive celler mellem behandlings- og PBS-grupperne, blev en non-parametrisk Kruskal-Wallis test udført. Dernæst blev en regionvis sammenligningsanalyse (Mann-Whitney U test) udført og præsenteret ved hjælp af volcano-plots for at undersøge forskellene i hjerneregionernes c-Fos positive celler mellem behandlings- og PBS-grupperne.

Resultater:

Mann-Whitney U-testen viste ingen signifikant forskel i hele hjernens c-Fos positive celleantal mellem de ubehandlede naive og SNI-mus, men på hjerne regionsniveau blev der observeret nogle få forskelle. Kruskal-Wallis-testen viste en signifikant ($p < 0,05$) forskel mellem morfin og mPD5 for både naive og SNI-mus (SNI $p = 0,0014$ and naive $p = 0,023$) samt en signifikant ($p < 0,05$) forskel mellem morfin og PBS i både naive og SNI-mus (SNI $p = 0,007$ and naive $p = 0,0002$). Volcano plotsene viste, at mPD5 inducerede aktivitet i hjerneregioner, der processerer nociceptive informationer.

Konklusion:

Denne undersøgelse demonstrerede de aktivitetsinducerende effekter af mPD5 i hjerneregioner, der processerer nociceptive informationer. Desuden viste den, at mPD5 har langt mindre aktivitetsinducerende effekt på hjernen sammenlignet med morfin og ser ikke ud til at præsentere de samme afhængighedsskabende egenskaber som morfin. Dette tyder på, at mPD5 repræsenterer en lovende lægemiddelkandidat til videre præklinisk testning, før den går videre til kliniske forsøg og behandling af neuropatisk smerte.

Acknowledgement

I would like to express my gratitude to my supervisor, Kenneth Lindegaard Madsen for the extremely helpful support and guidance he provided during my time under his supervision in the writing process. Moreover, I would like to thank Sara Jager for her invaluable daily support in the laboratory and imaging facility. Both shared knowledge, answered my questions and provided constructive feedback which has been very valuable throughout my research. I would also like to thank Grace Anne Houser for helping me with the data analysis. The trust and confidence they have had in me throughout our collaboration is highly appreciated. I look forward to applying the knowledge and skills I have gained under their guidance in my future work.

In extension, I would like to express my sincere gratitude to my internal supervisors Kristian Kjær Pedersen and Maj Schneider for their guidance. They have always been available despite my work being done in Copenhagen. They have steered me in the right direction and made sure that my work adheres to the necessary standards.

List of abbreviations

ACC: Anterior cingulate cortex
AMG: Amygdala
AMPA: Amino-3-hydroxy-5-methyl-4-isoxazolepropionic acid
ATP: Adenosine triphosphate
AUDpol: Posterior auditory area, layer 1
CI-AMPA: Ca^{2+} -impermeable receptor
CL: Central lateral nucleus of the thalamus
CNS: Central nervous system
COPY: Copula pyramidis
CP-AMPA: Ca^{2+} -permeable receptor
DCM: Dichloromethane
DNIC: Diffuse noxious inhibitory control
DMSO: Dimethylsulfoxid
DRG: Dorsal root ganglion
ECi: Ethyl-3-phenylprop-2-enoate
fMRI: Functional magnetic resonance imaging
FRP5: Frontal pole, layer 5
IAD: Interanterodorsal nucleus of the thalamus
MOs5: Secondary motor area, layer 5
MOs6a: Secondary motor area, layer 6a
MOp6a: Primary motor area, layer 6a
mPD5: Myr-NPEG₄-(HWLKV)₂
MQ-water: Milli-Q-water
NAcsh: Nucleus accumbens
NIH: US National Institute of Health
NNT: Numbers needed to treat
PAG: Periaqueductal grey
PB: Parabrachial nucleus
PBS: Phosphate buffered saline
PDH: Pyruvate dehydrogenase
PFA: Paraformaldehyde
PFC: Prefrontal cortex
PICK1: Protein interacting with C kinase - 1
PL2/3: Prelimbic area, area 2/3
PNS: Peripheral nervous system
PP: Peripeduncular nucleus
pPDH: Phosphorylation of pyruvate dehydrogenase
PPY: Parapyramidal nucleus
PRE: Presubiculum
QoL: Quality of life
RE: Nucleus of reuniens
RI: Refractive index
RSPagl6b: Retrosplenial area, lateral agranular part, layer 6
RVM: Rostral ventral medulla
S1: Somatosensory cortex

SNI: Spared nerve injury
SPVC: Spinal nucleus of the trigeminal caudal part
SSp-ll1: Primary somatosensory area, lower limb, area 1
SSp-ll2/3: Primary somatosensory area, lower limb, area 2/3
SSp-ll4: Primary somatosensory area, lower limb, area 4
SSp-ll5: Primary somatosensory area, lower limb, area 5
SSp-tr4: Primary somatosensory area, trunk, area 4
SSp-m4: Primary somatosensory area, undefined area, layer 1
SSp-un1: Primary somatosensory area, mouth, layer 1
TCA: Tricarboxylic cycle
TMd: Tuberomammillary nucleus, dorsal part
VISC1: Visceral area, layer 1
VISC2/3: Visceral area, layer 2/3
VTA: Ventral tegmental area
3D: Three-dimensional

Table of content

Introduction	1
<i>Chronic pain as a major global issue</i>	<i>1</i>
<i>Treatment of neuropathic pain.....</i>	<i>1</i>
<i>The analgesic effects of morphine.....</i>	<i>2</i>
<i>The four stages of pain.....</i>	<i>3</i>
<i>The pain matrix.....</i>	<i>4</i>
<i>Neuropathic pain</i>	<i>5</i>
<i>Glutamatergic neurotransmission and subunit specific AMPAR trafficking in central sensitization.....</i>	<i>6</i>
<i>mPD5 as a new treatment strategy for neuropathic pain.....</i>	<i>7</i>
<i>Animal model for preclinical assessment of pain.....</i>	<i>10</i>
<i>Detection of neuronal activity and inhibition for preclinical assessment of pain</i>	<i>11</i>
<i>Tissue-based clearing and 3D whole-brain imaging</i>	<i>12</i>
<i>Problem delimitation.....</i>	<i>13</i>
<i>Study aim.....</i>	<i>13</i>
<i>Hypothesis.....</i>	<i>13</i>
Method.....	14
<i>In vivo</i>	<i>14</i>
Animals	14
Spared nerve injury model	15
Von Frey Measurements: Mechanical Pain Threshold.....	15
Drug administration and dosing	16
Tissue collection.....	16
<i>Tissue clearing.....</i>	<i>18</i>
Bleaching	18
Immunolabeling	19
Clearing.....	20
<i>Imaging.....</i>	<i>20</i>
Microscope setup.....	20
Image acquisition	21
Whole-brain c-Fos quantification.....	21
Results.....	22
<i>The supraspinal expression of c-Fos is not changed in the non-treated SNI mice.....</i>	<i>22</i>
<i>The c-Fos expression changed after morphine administration in naive and SNI mice</i>	<i>24</i>
<i>c-Fos expression changes in brain regions processing nociceptive information after mPD5 and morphine administration in the naive and SNI cohorts.....</i>	<i>27</i>
Morphine vs PBS	27
mPD5 vs PBS.....	31
<i>Unsuccessful staining with a pPDH antibody as a proxy for neuronal inhibition</i>	<i>34</i>
Discussion	36

<i>The supraspinal effects of the SNI model</i>	<i>36</i>
<i>The analgesic effects of morphine and mPD5</i>	<i>37</i>
Morphine	37
mPD5	39
<i>Consideration for the employment of pPDH in future immunolabeling studies.....</i>	<i>41</i>
<i>Limitations</i>	<i>41</i>
Conclusion	42
References	44
Appendices	58
<i>Appendix 1: Protocol for tissue clearing and immunolabeling.....</i>	<i>58</i>
<i>Appendix 2: total c-Fos positive cells detected in the SNI mice for each brain in the three different groups: PBS, morphine, mPD5</i>	<i>63</i>
<i>Appendix 3: total c-Fos positive cells detected in the naive mice for each brain in the three different groups: PBS, morphine, mPD5</i>	<i>63</i>
<i>Appendix 4: Data from the naive morphine-treated and PBS-treated cohort</i>	<i>64</i>

Introduction

Chronic pain as a major global issue

Pain perception is a fundamental part of avoiding danger and staying alive, however when pain persists beyond tissue healing and no longer serves a protective biological function, the pain becomes pathological (Cohen & Mao, 2014). The International Association for the Study of Pain defines chronic pain as “pain that persists or recurs for longer than three months, with biological, psychological and social factors contributing to the syndrome” (*WHO*. 2021). Chronic pain has a significant impact on quality of life (QoL) affecting family life, social life, physical functioning, and professional life. Globally, 20% of adults are suffering from chronic pain, of which a fifth of people are thought to have a subtype of chronic pain, neuropathic pain (Cohen & Mao, 2014; Finnerup et al., 2018). Neuropathic pain is caused by lesions to the somatosensory system, which alter the function and structure of pain, so that the response to pain occurs spontaneously and the perception of innocuous and noxious stimuli are pathologically strengthened (COSTIGAN et al., 2009).

Several diseases and factors can lead to the development of neuropathic pain, including viral infections, diabetes, chemotherapy, surgical procedures, or mechanical compression of nerves. Despite the high prevalence of neuropathic pain, the pathophysiological mechanisms remain poorly understood, why the development of effective treatments are limited. (Finnerup et al., 2018)

Treatment of neuropathic pain

Neuropathic pain is a condition that has proven difficult to treat, and the current treatment options for neuropathic pain have performed poorly and with low efficacy. A systematic review by Finnerup et al., (2018) investigated factors associated with decreases in drug efficacy and demonstrated that the numbers needed to treat (NNT) for most neuropathic pain drugs is 5-7 persons. Thus, only a minority of people with severe neuropathic pain respond to the medication and achieve meaningful pain relief. (Finnerup et al., 2018) Second- and third-line treatment for neuropathic pain are opioids, even though 21-29% of patients misuse prescribed opioids, and 8-10% of these patients develop an opioid addiction. Despite the low efficacy of opioids, neuropathic pain patients are still prescribed these medications. (Vowles et al., 2015) See *table 1*, for a summary of the treatment regimen for neuropathic pain.

The negative impact on QoL, the high number of people suffering from neuropathic pain and the lack of sufficient treatment options highlight the need to develop more effective, non-addictive treatments for neuropathic pain.

Table 1. Treatment regimen of neuropathic pain according to “The special interest Group” on Neuropathic Pain (WHO, 2021)

Treatment regimen for neuropathic pain		
First line	Gabapentinioids	Tricyclic antidepressants
Second line	Opioids (Tramadol)	Topical treatment
Third line	Opioids (Morphine)	

The analgesic effects of morphine

The second- and third-line drugs for neuropathic pain include opioids, both strong (e.g., morphine) and weak (e.g., tramadol). Morphine exerts its effect by binding to the endogenous μ -opioid G-coupled receptors, which are found in areas such as the thalamus, the ventral tegmental area (VTA), rostral ventral medulla (RVM), periaqueductal gray (PAG) and in the dorsal horn of the spinal cord. When morphine binds to its receptors, it activates inhibitory G_i -coupled intracellular pathways. The activation leads to the closing of voltage-sensitive calcium channels and potassium efflux, reducing neuronal excitability. Pain transmission in the dorsal horn is reduced by inhibiting the release of excitatory neurotransmitters and causing postsynaptic hyperpolarization. In the brain, morphine enhances descending inhibition through PAG, stimulating the descending inhibitory pathways of the central nervous system (CNS) and inhibiting nociceptive afferent neurons of the peripheral nervous system (PNS), thus reducing pain transmission. (Cooper et al., 2017)

Although morphine is known for its analgesic effects, it has proved to cause substance use disorder in some patients (Listos et al., 2019). Brynildsen et al., (2020) showed that repeated exposure to morphine in mice leads to reorganization of neuronal circuitry, potentially causing addiction-associated behaviors. Additionally, morphine targets dopamine neurons in a component of the brain's reward system called the VTA, by inhibiting interneurons in the VTA (Brynildsen et al., 2020). This inhibition allows the activation of the dopamine neurons in the VTA, which can ultimately lead to addiction-associated behaviors (Chen et al., 2015). Another study by Alok, (2021) characterized the progression of morphine-induced behavioral tolerance in rats in an open field test. This study found that the motor behaviors (speed, moving time, distance travelled) were suppressed

30 minutes post-morphine injections, whereafter an increase in the parameters were seen 10 days after repetitive morphine treatment, indicating tolerance. (Alok, 2021)

The four stages of pain

Pain pathways are complex sensory systems activated to provide a protective response to noxious stimuli. The pain pathway can be divided into four processes: transduction, transmission, modulation, and perception. **Transduction** begins when a peripheral noxious stimulus is detected by specialized noxious ion channels of two main groups of primary afferent nerve fibers: myelinated A-fibers and unmyelinated C-fibers. A-fibers transmit a faster signal to the spinal cord due to their myelinated axons and initiates a highly localized sharp sensation as a first response to noxious stimulus. The C-fibers deliver a more diffuse, burning sensation and transmit a slower signal to the spinal cord compared to A-fibers. Both A-fibers and C-fibers (known as first-order neurons) have their cell bodies in the dorsal root ganglion (DRG) and in the trigeminal ganglion, both part of the PNS. (Osterweis et al., 1997) During **transmission**, the action potential generated from the free nerve endings of A and C-fibers propagates from the PNS to the CNS along primary afferent axons. The axons synapse in the dorsal horn of the spinal cord with second-order neurons. From the second-order neurons, the signal is transmitted to the brain via the spinothalamic tract. The axons of the second-order neurons decussate before ascending to the brain in the lateral and anterior spinothalamic tract. (Osterweis et al., 1997) **Modulation** occurs throughout the entire nociceptive transmission pathway, including the primary afferent neurons, the dorsal horn, and in the higher brain regions. Modulation is relevant for pain signaling and perception. Modulation of the descending pathways is required to sufficiently inhibit pain perception, although this pathway is deficient in many chronic pain patients. This deficiency can be measured by the loss of diffuse noxious inhibitory controls (DNIC), as previously measured by Patel & Dickenson, (2020), who assessed deficits in endogenous pain modulation in neuropathic rats by the loss of DNIC. **Perception** is the final process where all information is integrated and processed in the cerebral cortex through third-order neurons projecting from the thalamus to higher brain regions, leading to the perception of pain. (Osterweis et al., 1997)

The pain matrix

Pain is not synonymous with nociception, as nociception can trigger brain responses without causing pain perception. Conversely, pain can occur without nociceptive input. (Legrain et al., 2011) The complexity of how the cortex processes nociceptive inputs has been investigated in humans through functional magnetic resonance imaging (fMRI) (Apkarian et al., 2005; Geuter et al., 2020; Lindquist et al., 2017). This technique has shown that nociceptive stimuli elicit responses in cortical networks consisting of the affective-motivational and sensory-discriminative networks, also referred to as the “pain matrix” (Legrain et al., 2011), illustrated in *figure 1*. The sensory-discriminative network (lateral part of the spinothalamic tract) includes the somatosensory cortices (S1/S2). The S1 region is associated with identification of different aspects of touch (size, shape, texture), and the S2 region is associated with tactile and spatial memory. Additionally, this pathway includes the prefrontal cortex (PFC). The affective-motivational pathway (anterior part of the spinothalamic tract) includes the parabrachial nucleus (PB) and amygdala (AMG). The AMG conveys signals to the anterior cingulate cortex (ACC), VTA, nucleus accumbens (NAch) and insula cortex, all of which are part of the mesolimbic system associated with regulation of emotional and motivational responses. All these areas are relevant for the complexity and heterogeneity of pain, as affect, sensation, and cognition contribute to the pain experience (Yang, S. & Chang, 2019). Treating the “pain matrix” as a general system has been questioned, as pain processing regions have been defined in different ways. These include recording local field potentials using brain computer interface (Sun et al., 2023), using fMRI (Reddan & Wager, 2018) and invasive neurophysiological recordings (Singh et al., 2020). Additionally, applying a high-dimensional mediation analysis to study the relationship between stimulus intensity and pain has also been demonstrated (Geuter et al., 2020). Despite the use of different techniques to assess which brain regions process pain, there is consensus on some brain regions associated with processing nociceptive information (Legrain et al., 2011; Reddan & Wager, 2018; Singh et al., 2020; Sun et al., 2023). These brain regions are illustrated in *figure 1*.

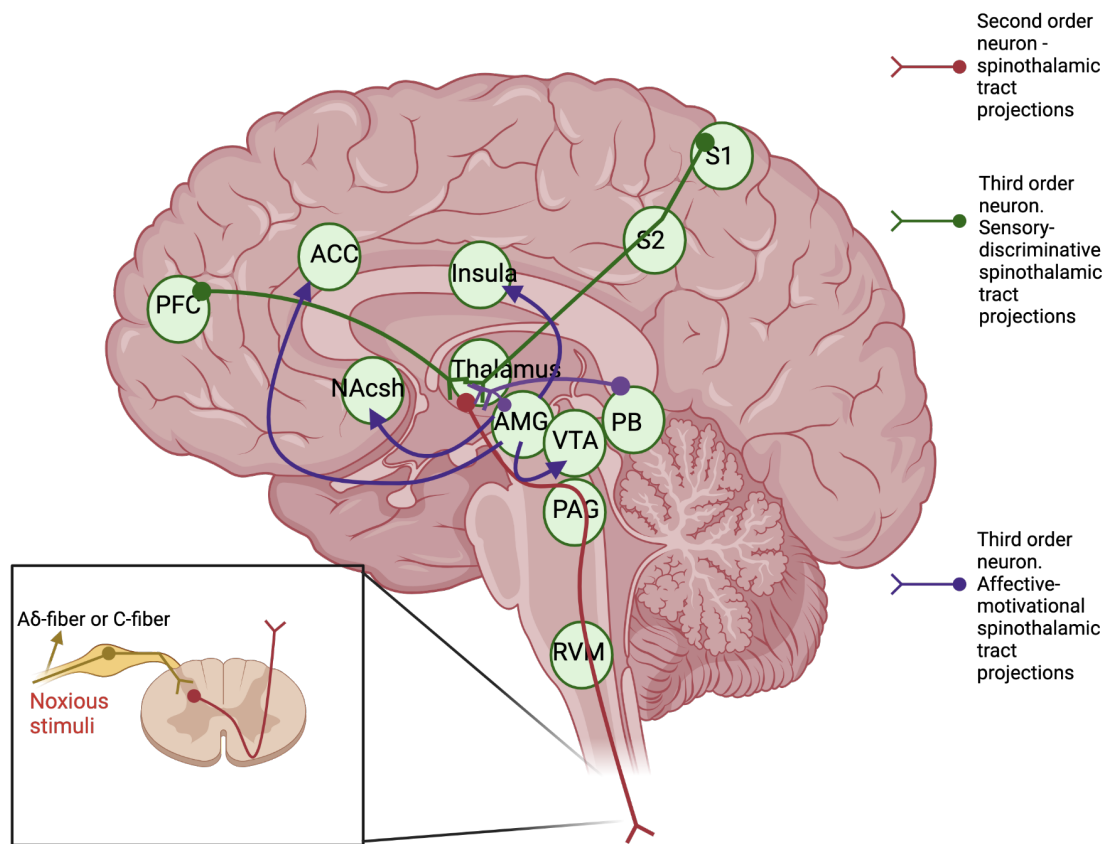


Figure 1. Ascending projections for the “Pain Matrix”. Adapted from (C. Reddan et al. 2018)

A simplified overview of the brain targets of the nociceptive pathway (red) and its lateral (purple) and anterior (green) pathways in the brain.

A noxious stimulus triggers either Aδ-fibers or C-fibers which synapse with second-order neurons in the dorsal horn, from where it decussates the midline. The signal will ascend either laterally or anteriorly via the spinothalamic tract (red) to the brain. Third-order neurons in the thalamus will transmit the signal to the somatosensory cortex (S1 and S2) and prefrontal cortex (PFC) via the sensory discriminative spinothalamic tract projections (green) as well as signals to parabrachial nucleus (PB) and amygdala (AMG) via the affective-motivational spinothalamic tract projections (purple). The amygdala will further convey signals to the anterior cingulate cortex (ACC), ventral tegmental area (VTA), nucleus accumbens (NAch) and insular cortex (purple). Created using Biorender.com.

Neuropathic pain

The pathophysiology underlying neuropathic pain involves both central and peripheral sensitization. Sensitization leads to a strengthened response to incoming signals by primary afferent nerve fibers and neurons in the CNS. Structural plasticity occurring after repeated or intense noxious stimuli can sensitize the central nociceptive system, producing hypersensitivity under pathological and normal

situations. Once sensitization has occurred, the CNS alters how it responds to sensory inputs, generating a pain response due to plastic changes within the CNS rather than reflecting the presence of a peripheral noxious stimulus. (Latremoliere & Woolf, 2009)

The effect of the plastic changes leads to an increased membrane excitability, synaptic efficacy, or reduced inhibition throughout the nociceptive pathways. This results in symptoms such as hyperalgesia and allodynia, which typically present in neuropathic pain conditions. Allodynia makes previously non-painful sensory stimuli become painful, while hyperalgesia causes an increased pain sensation from a peripheral painful stimulus. (Siddall et al., 2003)

Both hyperalgesia and allodynia rely on the status of the descending pain control, which is regulated by the balance between descending facilitation and inhibition (Arendt-Nielsen et al., 2015). Descending pain control is usually deficient in chronic pain patients and can be measured via experimental conditioning pain stimuli in humans, where test stimulus is followed by a conditioning stimulus (one noxious stimulus is used to inhibit another noxious stimulus). Impaired descending pain modulatory pathways are potentially contributing to the development and maintenance of chronic pain conditions. (Ramaswamy & Wodehouse, 2021)

Glutamatergic neurotransmission and subunit specific AMPAR trafficking in central sensitization

Glutamate is an excitatory neurotransmitter in the CNS. One of its receptors, activated selectively by amino-3-hydroxy-5-methyl-4-isoxazolepropionic acid (AMPA), has been found to participate in synaptic plasticity, including central sensitization. Central sensitization is a phenomenon leading to excessive pain perception in neuropathic pain conditions. (Tao, 2012) In adult mice brains, most AMPA receptors are Ca^{2+} -impermeable (CI-AMPA) (Cull-Candy & Farrant, 2021). During persistent pain conditions, a higher expression and trafficking of Ca^{2+} -permeable AMPARs (CP-AMPA) in the pre- and post-synaptic plasma membranes has been demonstrated by Kopach et al., (2011). The behavior of AMPARs is regulated by the receptor's subunit composition, which can vary across brain regions and change in response to neuronal activity. One of the AMPARs subunits, GluA2, is important for subunit-specific trafficking of the AMPARs in central sensitization, as it renders AMPARs impermeable to Ca^{2+} . When intense noxious stimuli from primary nociceptive afferents reach the neuronal synapse, a phosphorylation of GluA2 on the CI-AMPA increases their affinity for the scaffold protein interacting with C kinase (PICK1). This

mediates endocytosis of the CI-AMPARs in vesicles, allowing CP-AMPARs to be freely trafficked to the synapse. The trafficking of CP-AMPARs to the synapse ultimately leads to an increased pain perception. (Cull-Candy & Farrant, 2021) Therefore, blocking PICK1 could decrease the excessive insertion of CP-AMPARs in the plasma membrane of neuronal synapses (Jensen et al., 2023).

mPD5 as a new treatment strategy for neuropathic pain

The third-line treatment option for patients with neuropathic pain is strong opioids (Vowles et al., 2015). Strong opioids, such as morphine, are prescribed despite dose-limiting side effects and severe impacts on the patients' QoL (Kang et al., 2023)

A new treatment for neuropathic pain has been developed which involves targeting specific scaffold proteins to modulate receptor trafficking (Christensen et al., 2020; Jensen et al., 2023). The increasing understanding of how maladaptive plasticity regulates subunit-specific AMPAR trafficking has led to the development of a new drug, myr-NPEG₄-(HWLKV)₂ commonly referred to as mPD5. This new drug is an inhibitor of PICK1, which targets the protein responsible for the insertion of excess CP-AMPARs. (Sørensen et al., 2022) An illustration of mPD5 can be seen in *figure 2a* and the proposed function of mPD5 is illustrated in *figure 2b*.

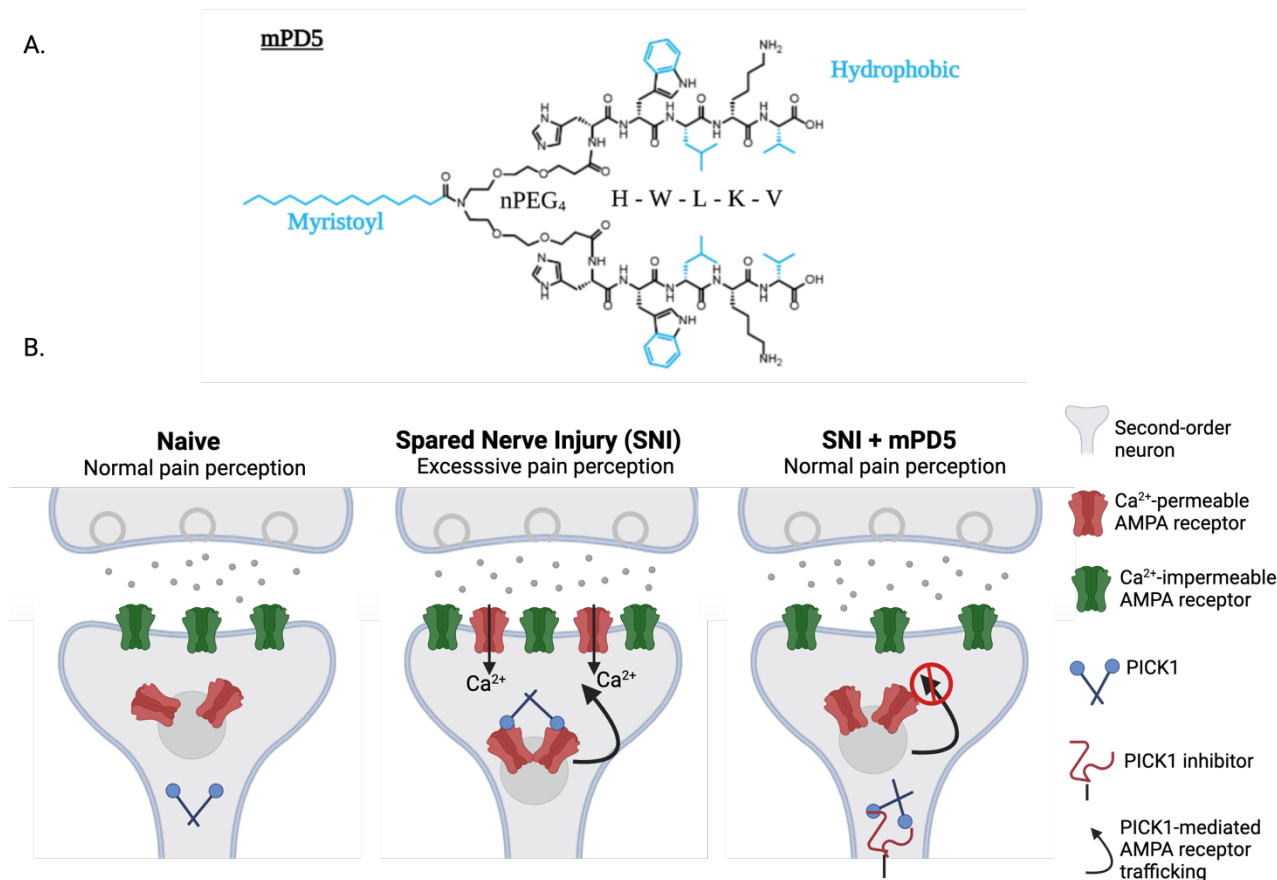


Figure 2. The chemical structure and function of mPD5. Adapted from (Sørensen et al., 2022)

A. The chemical structure of mPD5 with a PDZ-binding pentapeptide part consisting of the C-terminus five residues of the dopamine transporter (D5) with a nPEG₄ linker as well as a C₁₄ fatty acid, myristoyl. Blue structures are hydrophobic.

B. Illustration of the proposed mechanism of action for mPD5. In B (left) there is a normal pain perception and CI-AMPA receptors are present in the plasma membrane. In B (middle) central sensitization occurred, with an excess insertion of CP-AMPA receptors due to PICK1-mediated AMPA receptor trafficking, which will lead to excessive pain perception. In B (right) mPD5 blocks protein interacting with C kinase 1 (PICK1) and prevents PICK1-mediated AMPA receptor trafficking and thereby normalizing the pain perception. Created using Biorender.com.

mPD5 is a bivalent pentapeptide inhibitor of PICK1 with high affinity to the PDZ-domain of PICK1. The pentapeptide part is the C-terminus of the dopamine transporter D₅, and the two separate pentapeptide parts are conjugated via an NPEG₄-linker. To enhance cell permeability, plasma stability, distribution, and reduce potential side effects, a fatty acid (myristoyl) is added. (Jensen et al., 2023)

PICK1 is found in glutamatergic neurons in the postsynaptic density in the DRGs and lamina I and II of the dorsal horn in the spinal cord, which are areas important for nociceptive transmission (Atianjoh et al., 2010). Moreover, Jensen et al., (2023) found PICK1 to be involved in thermal and mechanical hypersensitivity in neuropathic pain models. Based on this theory, PICK1 stabilizes GluA2 of AMPARs, resulting in the internalization of CP-AMPA, as illustrated in *figure 2B(middle)*. To prevent this from happening, Christensen et al., (2020) found that inhibition of PICK1 reduces the interaction between PICK1 and the GluA2 subunit of AMPARs, as illustrated in *figure 2B(right)* which reduces the internalization of CP-AMPA.

No data has yet proven the entry of mPD5 into the brain, although its pain-relieving properties have shown promising results (Christensen et al., 2020; Jensen et al., 2023). Jensen et al., (2023) demonstrated advantageous pharmacodynamic properties and relief of evoked and ongoing mechanical hypersensitivity following subcutaneous administration of mPD5 in an inflammatory pain model. The same study showed that mPD5 relieved mechanical hyperalgesia in a spared nerve injury (SNI) rodent model, lasting up to 20 hours after repeated administration (Jensen et al., 2023). Additionally, Christensen et al., (2020) used two neuropathic pain models (SNI and streptozotocin model) to show that inhibition of PICK1 dose-dependently relieves mechanical hyperalgesia and thermal hypersensitivity without affecting basal locomotion in naive mice in an open field test.

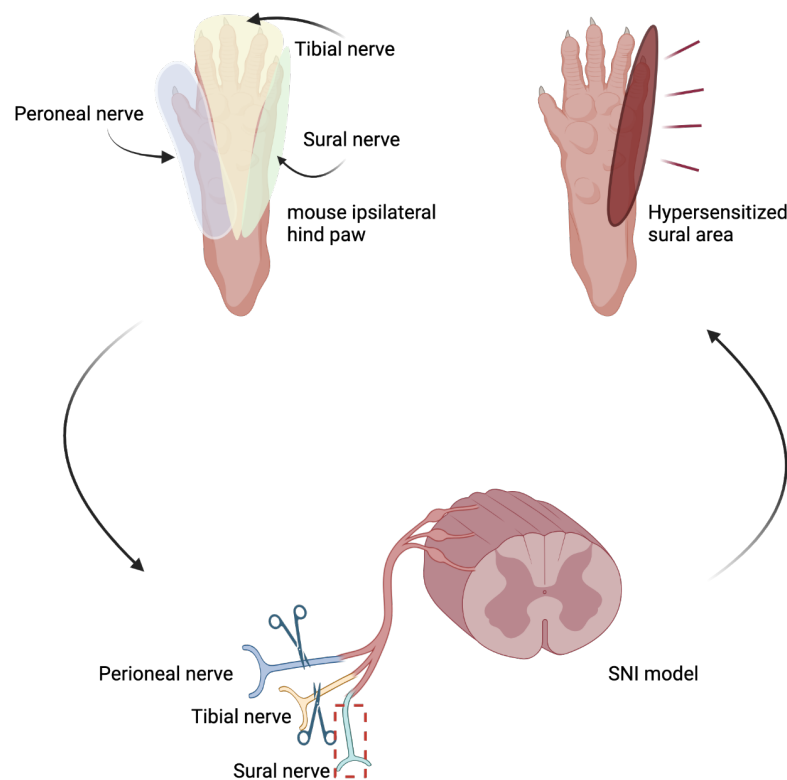


Figure 3. Spared nerve injury model of neuropathic pain. Adapted from (Duraku et al., 2012)

The three branches of the sciatic nerve innervate different areas of the plantar surface of the hind paw. The peroneal nerve innervates the medial part of the plantar surface (blue), the tibial nerve innervates the central part of the plantar surface (yellow), and the sural nerve innervates the most lateral part of the plantar surface (green). During the surgical procedure the peroneal nerve and the tibial nerve are transected, and the sural nerve is left intact, leading to a hypersensitized sural area. Created using Biorender.com.

Animal model for preclinical assessment of pain

Mimicking clinical neuropathic pain symptoms, such as thermal and mechanical pain hypersensitivity in rodent models, has previously been done using the surgical method SNI (Duraku et al., 2012; Guida et al., 2020; Shields et al., 2003). The SNI model involves dissecting two of the three branches of the sciatic nerve (the common peroneal nerve and the tibial nerve) in one hind paw, leaving the sural nerve intact, as illustrated in *figure 3*. The three branches of the sciatic nerve innervate areas of the hind paw: the tibial nerve innervates the center paw area, the common peroneal nerve innervates the medial area, and the sural nerve innervates the lateral part of both the dorsal and plantar surface of the paw. Transecting the peroneal and tibial nerves makes the area innervated by the sural nerve hypersensitive. (Shields et al., 2003) Guida et al., (2020) found that mice exhibit sensory symptoms such as hyperalgesia and allodynia following SNI surgery,

mimicking a neuropathic pain condition. Shields et al., (2003) assessed mechanical and thermal pain hypersensitivity by behavioral tests (Von Frey and Hargreaves), providing information on the mechanisms responsible for stimulus-evoked pain in neuropathic pain conditions.

Detection of neuronal activity and inhibition for preclinical assessment of pain

Studying the mechanism of drug effects for neuropathic pain in human neuroimaging studies has been challenged by the poor translatability of preclinical to clinical pain results (Eisenach & Rice, 2022). This poor translatability is described by Eisenach & Rice, (2022) as being caused by the complex biopsychosocial and individual experience of chronic pain and the lack of scientific progress. For the measurement of drug efficacy in rodents, most preclinical pain research relies on the behavioral responses. These responses have been investigated using the mouse grimace scale to assess pain in mice when subjected to an evoked painful stimulus (Glick et al., 2010), and the open field test to assess locomotor activity levels and anxiety in mice (Christensen et al., 2020).

However, measuring behavioral signs of spontaneous pain has proven difficult (Guida et al., 2020). The use of rodents to test for drug efficacy is supported by the US National Institute of Health (NIH), who concluded that high throughput screening of novel analgesics should be performed and evaluated in rodents before moving on to further testing (Domínguez-Olivia Adriana et al., 2023).

To identify brain regions affected by drug dependence, withdrawal, and reward, the immediate early gene c-Fos has been successfully used preclinically as a marker for neuronal activity in rodent models (Brynildsen et al., 2020; Hossaini et al., 2014; KOVACS, 2008). Brynildsen et al., (2020) have used c-Fos to identify brain regions associated with opioid exposure and found increased c-Fos expression in the ACC, NAc, and AMG. Another study by KOVACS, (2008) describes c-Fos as a good marker for neuronal activity within the CNS for several reasons: it is found in low expressions in the brain under basal conditions, it is induced in response to extracellular signals such as neurotransmitters and ions, and the response is transient. Additionally, Hossaini et al., (2014) managed to induce c-Fos expression in an SNI model in mice with a peak expression after 2 hours in the spinal cord.

Both morphine and mPD5 exert inhibitory effects by default (Cooper et al., 2017; Jensen et al., 2023). Therefore, investigating a surrogate representing the decrease of neuronal activity (inhibition) is interesting, although the literature on this is sparse. Yang, D. et al., (2023) tested the

phosphorylation of pyruvate dehydrogenase (pPDH) as a marker for inhibition. Pyruvate dehydrogenase (PDH) is part of the adenosine triphosphate (ATP) production in the tricarboxylic (TCA) cycle and is found in mitochondria (Lazzarino et al., 2019). Phosphorylation of PDH inhibits the enzymatic activity required for the ATP production in the TCA cycle, subsequently decreasing the production of ATP. Yang, D. et al., (2023) succeeded in staining with pPDH in an in vivo mouse model and detected neuronal inhibition across the brain, induced by natural behaviors and general anesthesia. While there is one suggestion of using pPDH as a marker for neuronal inhibition, the data supporting this claim is still limited. (Yang, D. et al., 2023)

Tissue-based clearing and 3D whole-brain imaging

For several decades, histological techniques have been the standard procedure for investigating tissues. However, a complete understanding of biological mechanisms in diseases requires not only selected parts of tissues but an unbiased exploration of the entire organ or organisms (Richardson et al., 2021). Several articles have used tissue clearing as a fast, robust, and unbiased approach to explore the neuronal activity in adult mice brains (Renier et al., 2014; Renier et al., 2016). Tissue clearing facilitates deep imaging of three-dimensional (3D) structures, enabling visualization of networks and spatial relationships between cell types in whole organs. The principle of tissue clearing is to achieve homogenization of refractive indexes (RI) throughout the tissue and remove endogenous absorbents without disruption of molecules of interest. The heterogeneity in RIs of tissue components contributes to light scattering and absorption, so tissue clearing is achieved through water removal (dehydration), pigment removal (depigmentation), and lipid removal (delipidation). Lastly, RI matching of the remaining dehydrated proteins allows optimal use of the light sheet microscope to obtain 3D data without light scattering. (Richardson et al., 2021)

Problem delimitation

Neuropathic pain is a global health issue, and current treatments are associated with dose-limiting and severe side effects, such as substance abuse. The NNT for first-line neuropathic pain treatments is high, underscoring the urgent need for novel therapeutic options. Recent research has demonstrated the pain-relieving properties of mPD5 in various behavioral rodent models, including those measuring mechanical pain (von Frey test), thermally evoked pain (Hargreaves test), and non-evoked pain (marble burying). However, the central effects of mPD5 remain insufficiently explored.

Existing approaches to assess drug targets and treatment effects utilize whole-brain 3D imaging, highlighting the necessity for unbiased methodologies to evaluate and quantify the therapeutic effects of analgesic drugs comprehensively. Consequently, the current study aims to investigate the supraspinal effects of mPD5 on a whole-brain scale as a potential new treatment for neuropathic pain.

Study aim

This study aims to compare the supraspinal effects of mPD5 to morphine in a mouse model of neuropathic pain on a whole-brain scale, assessed via the immediate early gene c-Fos as a proxy for neuronal activity. Utilizing tissue-clearing and immunolabeling techniques for optimal deep structure visualization, this project seeks to explore mPD5 as a promising alternative to opioids in the treatment of neuropathic pain.

Hypothesis

The hypothesis of this study will observe:

1. Significant differences in the c-Fos signal between the non-treated SNI and naive group.
2. Widespread response in the treatment of both SNI and naive mice with opioids compared to mPD5.
3. Significant changes in c-Fos activity in brain regions processing nociceptive information, as defined in *figure 1*, in both mPD5 and morphine-treated groups.

In addition, the current study worked on testing the staining protocol for pPDH as a proxy for neuronal inhibition on a whole-brain scale.

Method

In this section the method employed in all four experiments to acquire whole-brain cell counts from mice will be explained. Firstly, the in vivo part of the experiments will be outlined. Next, tissue clearing and immunolabeling will be explained and lastly the imaging of the cleared mouse brains will be accounted for, including the microscope setup and acquisition. An overview of the conducted experiments is illustrated in *figure 4*.

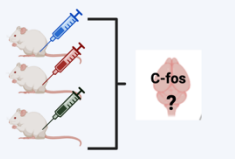
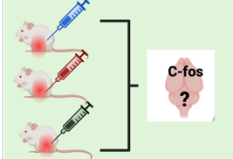
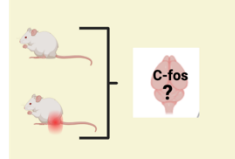
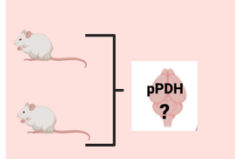
	Naive mice	SNI mice	Naive + SNI mice	Inhibition mice
Number of mice	24	24	14	12
Groups within each experiment	3 A 10 mg/kg morphine B 10 µmol/kg mPD5 C PBS	3 A 10 mg/kg morphine B 10 µmol/kg mPD5 C PBS	2 SNI Naive	2 Positive control - naive Control - 2 hours of 1.5% isoflurane
Gender of mice	Male	Male	Male	Male
Strain of mice	Wildtype C57BL/6NRj	Wildtype C57BL/6NRj	Wildtype C57BL/6NRj	Wildtype C57BL/6NRj
Purpose of experiment	Assess c-fos signal in naive mice post mPD5 and morphine treatment	Assess c-fos signal in SNI mice post mPD5 and Morphine treatment	Assess c-fos signal in naive + SNI mice without treatment	Assess pPDH signal in naive mice without treatment
				

Figure 4. Group overview and purpose of different experiments.

A color-coded overview over the 4 different experiments and the strain of mice; (1) naive (2) SNI (3) naive+SNI (4) inhibition. Furthermore, the figure illustrates the different groups within each experiment as well as the given treatments. The purpose of each experiment is briefly described, and brains will be imaged to detect the respective antibody signal. Blue syringe illustrates PBS, red syringe illustrates morphine and green syringe illustrates mPD5. The red mark on the hindleg of the mice marks SNI operated mice. Created using Biorender.com.

In vivo

Animals

74 8-week-old wild-type male C57BL/6NRj mice were brought from Janvier (n= 6-8 mice per treatment group). Upon arrival at the animal facilities of the Biological Institute of the University of Copenhagen, the mice were allowed 7 days of habituation before the start of the experiment. The

mice were group-housed in a temperature-controlled room with 12-h light/dark cycle with lights on from 6 am and had free access to water and standard rodent chow. Animal experiments were performed according to guidelines of the Danish Animal Experimentation Act (BEK no. 1018 of 14/12/2020) and conducted by authorized personnel with FELASA ABD in a fully AALAC-accredited facility. The Danish Animal Experimental Inspectorate under the Ministry of Food, Fisheries, and Agriculture approved the experiments (license no. 2016-15-0201-00976).

Spared nerve injury model

30 9-week-old mice underwent SNI surgery to mimic a neuropathic pain model, as previously demonstrated by Cichon et al., (2018) and Shields et al., (2003). SNI was performed on the left hindleg of the mice under isoflurane anesthesia (induction 3% and maintained at 2.5%). On the day of surgery and two days after, mice received 5 mg/kg carprofen (Carprosan vet, 0.03 mg/mL) as pain relief medication. During the surgical procedure, mice received 80 µL buprenorphine (Temgesic, 0.03 mg/mL) for pain relief. The surgical procedure began with an incision of the skin on the lateral surface between the hip and knee, followed by a drop of lidocaine (2.5 mg/mL) on the biceps femoris muscle as a fast-acting sedative. A lengthwise division of the biceps femoris muscle exposed the three branches of the sciatic nerve. The sural branch was left intact, while the peroneal and tibial branches were ligated with a single surgical knot and axotomized distally to the ligation. Wounds were closed with surgical clips, and animals were monitored daily for signs of stress or discomfort. In all cases, the animals recovered uneventfully.

Von Frey Measurements: Mechanical Pain Threshold

Before and after the SNI surgery, mice underwent a Von Frey test to determine whether they had developed neuropathic pain. The Von Frey test assessed the threshold for mechanical pain response by applying an increasing bending force with von Frey filaments. Although pain cannot be directly measured in rodents, nociception can be quantified using stimulus-evoked methods like the Von Frey test, as previously demonstrated (Cichon et al., 2018; Shields et al., 2003). The baseline Von Frey test was conducted 7 days before the SNI surgery, specifically before the first treatment injection (mPD5, morphine, PBS), and again 2 days after SNI surgery. The 9-week-old mice (n=30) were placed in plastic boxes (11.5 cm x 14 cm) on a wire mesh and allowed 20 minutes of habituation to get comfortable with the equipment. The mechanical pain thresholds of the mice were determined on both hind paws using von Frey filaments. The filaments used ranged from 0.04 to 2 gram-forces, applied to the frontolateral plantar surface of the hind paws innervated by the

sural nerve. Each filament was applied five times with resting periods between each application. The pain threshold was determined by a positive response in at least three out of five reactions in two consecutive filaments. A positive pain reaction was defined as flinching, paw licking, or a sudden paw withdrawal induced by a von Frey filament.

Drug administration and dosing

Drugs were administered to 9-week-old naive mice (n=24) and to the SNI mice (n=24) on day 7 post-SNI surgery. The SNI and naive mice were split into 3 groups (n=8/group). All mice were injected subcutaneously with a 27G syringe (Chirana T. injecta, CH27012). The first group received 3.5 mM morphine dissolved in saltwater (10mg/kg). The second group received 1.0 mM mPD5 dissolved in PBS (10 micromol/kg). The third group received PBS. All mice were injected once daily for 7 days.

Tissue collection

The naive and SNI mice were terminated exactly 2 hours after the last drug administration on day 7 because c-Fos protein expression peaks 1-3 hours after stimulus (Wu et al., 2006). Therefore, an administration scheme was made with 15-minutes intervals between each mouse for the last injection. The 15-minute intervals allowed for anesthetizing, perfusion, and fixating before the next mouse had to be terminated. The administration scheme is shown in *figure 5*. Naive and SNI mice were anesthetized with 3% isoflurane, and reflexes were checked before starting transcardiac perfusion to ensure appropriate anesthetic depth. An incision was made on the chest followed by incisions in the diaphragm along the rib cage. Two cuts through both rib cages were performed to fully expose the heart and lungs. A 25G infusion needle (Chirana T. injecta, CH25100) was inserted inside the left ventricle, and the saline perfusion was performed by manually pushing the syringe (20 mL) at a slow constant speed until the blood was flushed out. The perfusion procedure was repeated with 4% paraformaldehyde (PFA). The naive and SNI mice brains were dissected and post-fixated with 4% PFA (Sigma-Aldrich, 100496) for 24 hours at 4°C.

The purpose of experiment 3, involving 7 SNI mice and 7 naive mice, was to explore if the SNI surgery resulted in significant changes in the c-Fos signal in the brain compared to naive mice. Experiment 4 was conducted as a proof of concept, following the study by Yang, D. et al., (2023), which identified pPDH as a reliable marker for detecting neuronal inhibition. The current study wanted to replicate their findings by testing the staining ability of the pPDH inhibition antibody

using different concentrations and incubation times (see table 2). Experiment 3 and 4 did not require an administration scheme, as no treatments were given. In experiment 3, both naive and SNI mice were randomly anesthetized, perfused, and fixated following the same procedure as described for experiment 1 and 2. In experiment 4, the mice stained with the inhibition antibody were split in two groups, with three mice in each group. One group of mice received the anesthesia as in experiment 1 and 2, while the second group received 4% isoflurane until they fell asleep, followed by 1.5% isoflurane for 2 hours. The two hours of isoflurane were given to the second group as a positive control, based on the findings by Yang, D. et al., (2023), who detected neuronal inhibition induced by 2 hours of general anesthesia. Perfusion and fixation followed the same procedure described above.






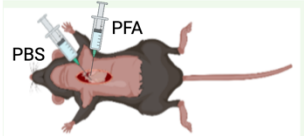
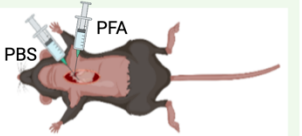

	Naive and SNI mice		
Total number of mice	48		
Groups	2x A	2x B	2x C
Number of mice	8	8	8
Treatment	PBS	10 mg/kg morphine	10 μ mol/kg mPD5
Time of 7th injection	0	+15 minutes	+30 minutes
 6 times			
Time of perfusion and fixation	+2 hours	+2 hours 15 minutes	+2 hours 30 minutes
 6 times			

Figure 5. Administration and termination scheme for naive and SNI mice in experiment 1 and 2. A group overview over the naive and SNI mice in experiment 1 and 2, and an administration scheme for their treatments as well as a termination scheme. Total number of mice for experiment 1 and 2 are 48 mice, with 24 mice in experiment 1 and 24 mice in experiment 2. Blue syringe illustrates PBS, red syringe illustrates morphine and green syringe illustrates mPD5. Created using Biorender.com.

Tissue clearing

To enable tissue clearing, the procedure previously demonstrated by Renier et al., (2014) was followed, allowing light sheet fluorescence microscopy of mice brains after PEGASOS and iDISCO+ based clearing and immunolabeling. This procedure was conducted on: (1) 24 naive mice, (2) 24 SNI mice, (3) 7 naive and 7 SNI mice, and (4) 12 naive mice, allowing investigation of brains in their 3D state. In the following section, the tissue clearing and immunolabeling of brains will be described. A timeline of the tissue-clearing process is provided in *figure*

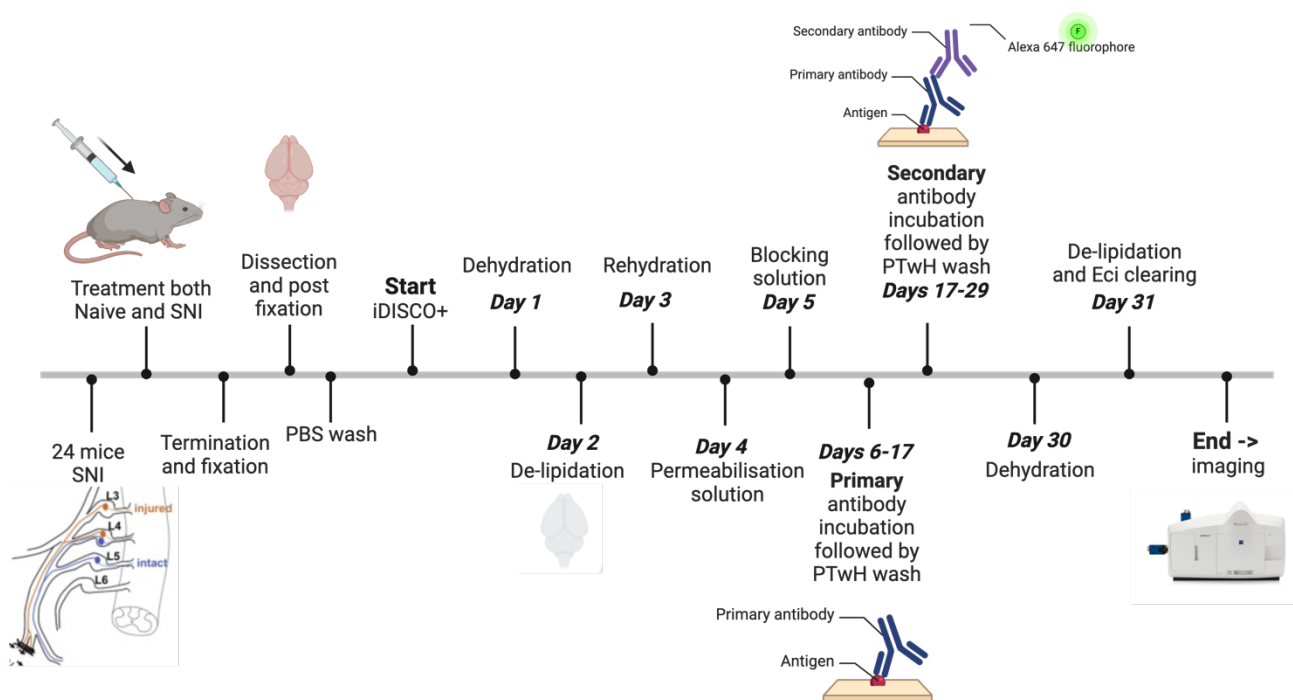


Figure 6. Timeline of tissue clearing and immunolabeling protocols.

Timeline of whole-brain clearing protocols and immunolabeling (iDISCO+). Firstly 24 mice underwent SNI surgery and subsequently both naive and SNI mice from experiment 1 and 2 received treatment. The brains were dissected and cleared following the iDISCO+ protocol. The brains were imaged on the Zeiss Light sheet 7 microscope. Created using Biorender.com.

Bleaching

The first step of tissue clearing was bleaching, which involves de-lipidation as well as decolorization of large pigments such as melanin and lipofuscin. Brains were incubated with 25% Quadrol (Sigma-Aldrich, 122262) in MQ-water for 3 days at 37°C. Quadrol was then replaced with

5% ammonium (fisher scientific, 64016) in MQ-water for 1 day at 37°C. After ammonium, dehydration was achieved in successive baths of MQ-water/methanol (20%, 40%, 60%, 80%, 2x100%, 1h each). Samples were then incubated with 5% hydrogen peroxide (H1009, sigma-Aldrich) in methanol (VWR, 85802.290) for 4 days with agitation at 4°C. After bleaching, rehydration was achieved in successive baths of MQ-water/methanol (80%, 60%, 40%, 20% methanol, 1h each). Four to five iterative washes with a washing buffer, PTwH (PTwH containing 1 L PBS: 11514526, Gibco[™], 2 mL tween 20: Sigma-Aldrich, G2500, 1 mL of 10mg/mL Heparin: Sigma-Aldrich, H3149, 2 mL 5% sodium azide in a 0,02% conc: Sigma-Aldrich, 71289) were done over 2-3 days.

Immunolabeling

To improve antibody penetration, samples were incubated with a permeabilization solution consisting of a washing buffer with 0.2% triton x-100 (Sigma-Aldrich, 11332481001) with the addition of 0.3M Glycine (Sigma-Aldrich, 410225) and 20% Dimethyl sulfoxide (DMSO) (Sigma-Aldrich, 276855) for 1 day under agitation at 37°C. To block unwanted antibody binding, the samples were incubated in a blocking solution with the same constituents as the permeabilization solution except the replacement of Glycine and DMSO with 1 g of 0.02% gelatin (Sigma-Aldrich, G2500) for 1 day under agitation at 37°C. Samples from naive and SNI mice were incubated with primary antibody rabbit anti-c-Fos (9F6) (cell signaling, 22505) in a 1:3000 concentration for 10 days and placed on an agitator at 37°C. Samples from the inhibition mice were incubated with primary antibody Phospho-Pyruvate Dehydrogenase α 1 (Ser293) (cell signaling #31866) at different incubation times and concentrations (see table 2) to test for optimal staining and placed on an agitator at 37°C. After the samples' respective days of incubation, the brains were washed with PTwH buffer for tissue blocks 3-4 times. They were then incubated with the secondary antibody Alexa flour 647 conjugated affinity-pure donkey anti-rabbit IgG, (Jackson immune research labs, NC0245384) in blocking solution at a 1:1000 concentration for 8 days and placed on an agitator at 37°C. Finally, the brains were washed with PTwH buffer for tissue blocks 3-4 times.

Table 2. An overview of the different concentrations and incubation times of the pPDH antibody given to 6 samples in experiment 4.

Phospho-Pyruvate Dehydrogenase α 1 (Ser293)		
	Incubation time	Concentration
Sample 1,4	14 days	1:500
Sample 3,6	14 days	1:250
Sample 2,5	7 days	1:250

Clearing

For sample clearing and preparation for imaging, the samples were dehydrated in successive baths of miliQ/methanol (20%, 40%, 60%, 80% and 100% methanol). They were then placed in a 2:1 Dichloromethane (DCM)/methanol (DCM, Sigma-Aldrich 34977) solution overnight for final delipidation. The samples were immersed twice in 100% DCM for 30 minutes each. Finally, the samples were placed in ethyl cinnamate (ECi) (Sigma-aldrich 800238) as the clearing agent to achieve a refractive index that matches the intracellular and extracellular fluids with the remaining dehydrated proteins in the samples.

Imaging

Microscope setup

The Zeiss Lightsheet 7 was used to image the mice brains due to its high speed, high resolution, and capability for deep imaging of transparent tissue (Pampaloni et al., 2015). The Lightsheet microscope was equipped with a 5x detection objective (EC Plan-Neofluar 5x, NA 0.16, working distance 18.5 mm) and sCMOS cameras (sCMOS pco.edge 4.2M). The Zeiss Lightsheet 7 has two illumination objectives (Zeiss LSM 5x/0.1 foc) to excite the samples' focal volume from both sides to avoid dispersion when scanning through the specimen. Lasers at 473-503 nm (30% power) were used for autofluorescence excitation, and lasers at 600-675 (60% power) were used to excite the fluorophore of the signal of interest. The lasers are fused into one illumination train. The emitted light first passes through a laser blocking filter to eliminate unwanted wavelengths, then through a second emission filter module that splits the remaining light above and below 560 nm into two cameras. The light below 560 nm passes through a band pass filter (505-545 nm) and is captured by the first camera as autofluorescence. Light above 560 nm is filtered by a longpass filter (660 nm) and captured by the second camera as the signal of interest. (Pampaloni et al., 2015)

Image acquisition

Image acquisition was managed using Zeiss Zen Black version 3.1 software. The brains were mounted on a sample holder with glue, suspended from above, allowing multiple mounting geometries while keeping the sample stationary during imaging. Brains were placed in ECi within a quartz cuvette (49x31x28 mm) in a transverse orientation. Tiling parameters were set with a 10% overlap between tiles, each consisting of 1280x1024 pixels. Most brains were covered with 4x6 tiles. The first and last image frames were set with a z-step size of 5 micrometers to achieve horizontal optical sectioning. The light-sheet and focal plane parameters were optimized to avoid misalignment, with the lightsheet thickness set to 10 micrometers and the exposure time set to 15 milliseconds. The Zeiss lightsheet 7 uses a pivot scan mode, allowing the angle of illumination to change during detection to avoid shadows in the field of view. Image time per brain is approximately 30 minutes.

Whole-brain c-Fos quantification

The tiled images from the Zeiss Lightsheet 7 were stitched using a custom Python script with TeraStitcher, developed by Bria & Iannello, (2012). The stitched images were further processed using ClearMap 2 software, a pipeline previously used by Fadahunsi et al., (2024). ClearMap 2 facilitates the depiction of c-Fos cell densities and region-wise cell count statistics through voxel map generation (Perens et al., 2021). The process in ClearMap 2 begins with images undergoing background removal. Next, cells are detected and assigned coordinates based on their volumes to eliminate smaller artifacts not depicted as cells. Autofluorescence images for each brain were aligned to the Gubra brain atlas using Elastix. The cell coordinates were then transformed to a reference coordinate space in the Gubra brain atlas. (Perens et al., 2021) The alignment of the light sheet scan to the Gubra brain atlas was manually inspected to ensure proper alignment by looking at the brains from the rostral to caudal end, illustrated in *figure 7*.

Voxel- and region-wise statistics between the 3 different experimental groups (SNI, naive and SNI+naive) were conducted using the SciPy application of the Mann-Whitney U test. Subsequently, volcano plots were generated to present regional c-Fos positive cell counts statistically.

Additionally, a non-parametric Kruskal-Wallis test followed by a Dunn's comparison test was performed on both the SNI cohort and naive cohort to compare the different treatment groups: mPD5, Morphine and PBS.

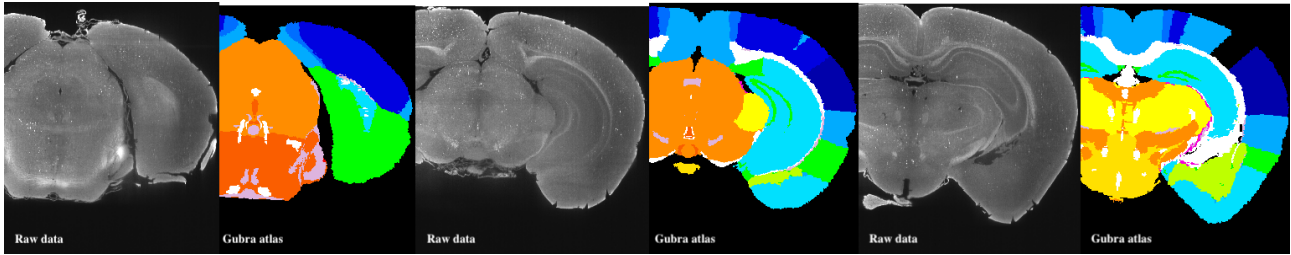


Figure 7. Alignment of a light sheet scan to the reference atlas, Gubra. The illustration shows different coronal z-stacks of morphine brain (B#5) with its respective coronal z-stack of the Gubra atlas. Pictures are taken from image j.

Results

Data on 24 SNI and 23 naive mice treated with either morphine, mPD5, or PBS will be presented together with data on 7 SNI and 6 naive non-treated mice. One brain from the naive mPD5-treated group and one brain from the SNI non-treated mice group were excluded due to destroyed tissue during imaging or dissection.

The supraspinal expression of c-Fos is not changed in the non-treated SNI mice

To assess if there were any supraspinal effects following the unilateral SNI surgery, non-treated naive and SNI mice were compared. Based on the Mann-Whitney U test, no statistically significant difference in total c-Fos positive cell counts was found between the non-treated SNI and naive mice, (*figure 8A*). The region-wise comparison of c-Fos positive cells showed that the SNI mice generally have fewer c-Fos positive cells in the cortical regions such as, primary somatosensory area, lower limb, area 2/3 (SSp-II2/3), secondary motor area, layer 5 (MOs5), presubiculum (PRE) and frontal pole, layer 5 (FRP5), compared to the naive cohort, (*figure 8B*).

The SSp-II2/3 region receives nociceptive information from the lower limb. This region had an average of 18 c-Fos positive cells detected in the SNI mice and an average of 34 c-Fos positive cells detected in the naive mice, (*figure 8C*). Brain regions such as visceral area, layer 1 (VISC1), and copula pyramidis (COPY) were found to have more c-Fos positive cells in the SNI cohort compared to the naive cohort, although the log2-fold change was not more than one, (*figure 8B*).

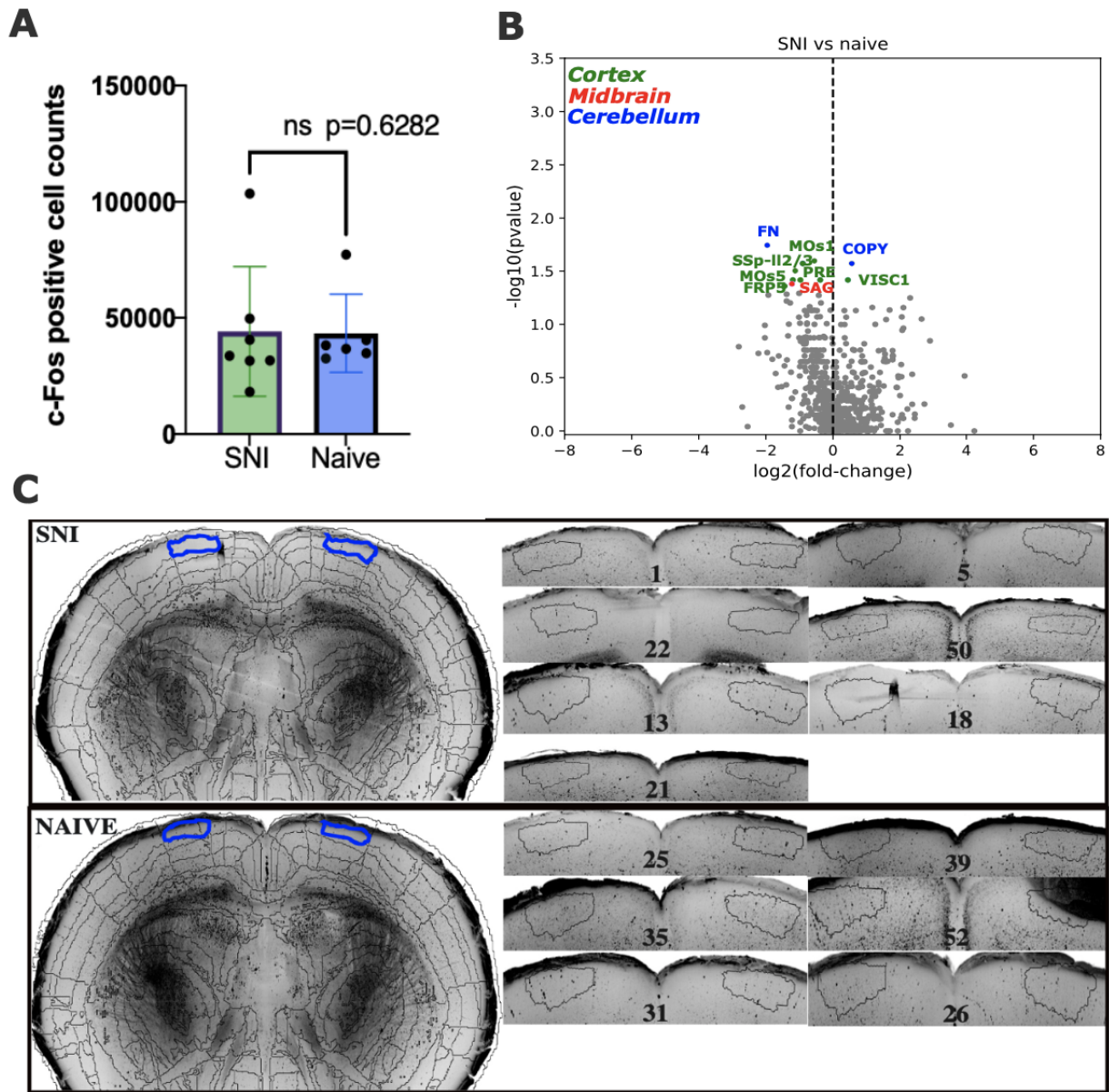


Figure 8. C-Fos expression in the brains of non-treated naive and SNI mice. Barplot (A), volcano plot (B) and optical sections (C), illustrating changes in c-Fos positive cells between non-treated naive and SNI mice. A. There is no change in total number of c-Fos positive cells in the SNI and naive mice. Data ($n=6-7$) are depicted as mean \pm SD and for the statistical analysis a Mann-Whitney U test was performed ($p=0.6282$). B. Anatomically colored volcano plot of non-treated SNI vs naive mice. The significant regions are divided into three anatomical regions: cortex (green), midbrain (red) and cerebellum (blue). The volcano plot shows regions with significant increase (right) or decrease (left) in c-Fos positive cell counts in the SNI group compared to the naive group. The x-axis represents the magnitude of difference of c-Fos positive cell counts from naive to SNI group. the y-axis represents the negative LogP-value. All dots represent a region of the mouse brain whereof the colored dots (red, green, blue) are the brain regions with significant ($p<0.05$) change in the number of c-Fos positive cells. C. Optical slices of raw data from the non-treated naive+SNI cohort. The SSsp-II2/3 brain region is highlighted in blue and shown for each mouse in the zoomed in panel. The SNI mice brains ($n=7$) are in the upper panel and the naive mice brains ($n=6$) are in the lower panel. The c-Fos positive cell count for the entire SSsp-II2/3 region is noted for every brain and the picture of each brain is represented by a single optical slice of 800 micrometers.

The c-Fos expression changed after morphine administration in naive and SNI mice

To assess the changes in c-Fos expression after morphine administration, optical slices of one morphine-treated, mPD5-treated, and PBS-treated brain were compared. No obvious difference in black dots were seen between the PBS and mPD5-treated mice, with each black dot representing a c-Fos positive cell, (*Figure 9*). In the morphine-treated brain, more c-Fos positive cells are seen compared to the optical slices of the PBS and mPD5-treated brains, (*Figure 9*). The morphine-treated brains have more than double the cell counts compared to the PBS and mPD5-treated brains. Specifically, the 8 SNI morphine-treated brains all showed a total of 107320 c-Fos positive cells, PBS-treated brains showed a total of 32325 c-Fos positive cells, and the mPD5-treated brains showed a total of 29986 cells, (see tables in Appendix 3 for the SNI cohort and Appendix 4 for the naive cohort on whole brain c-Fos positive cell counts).

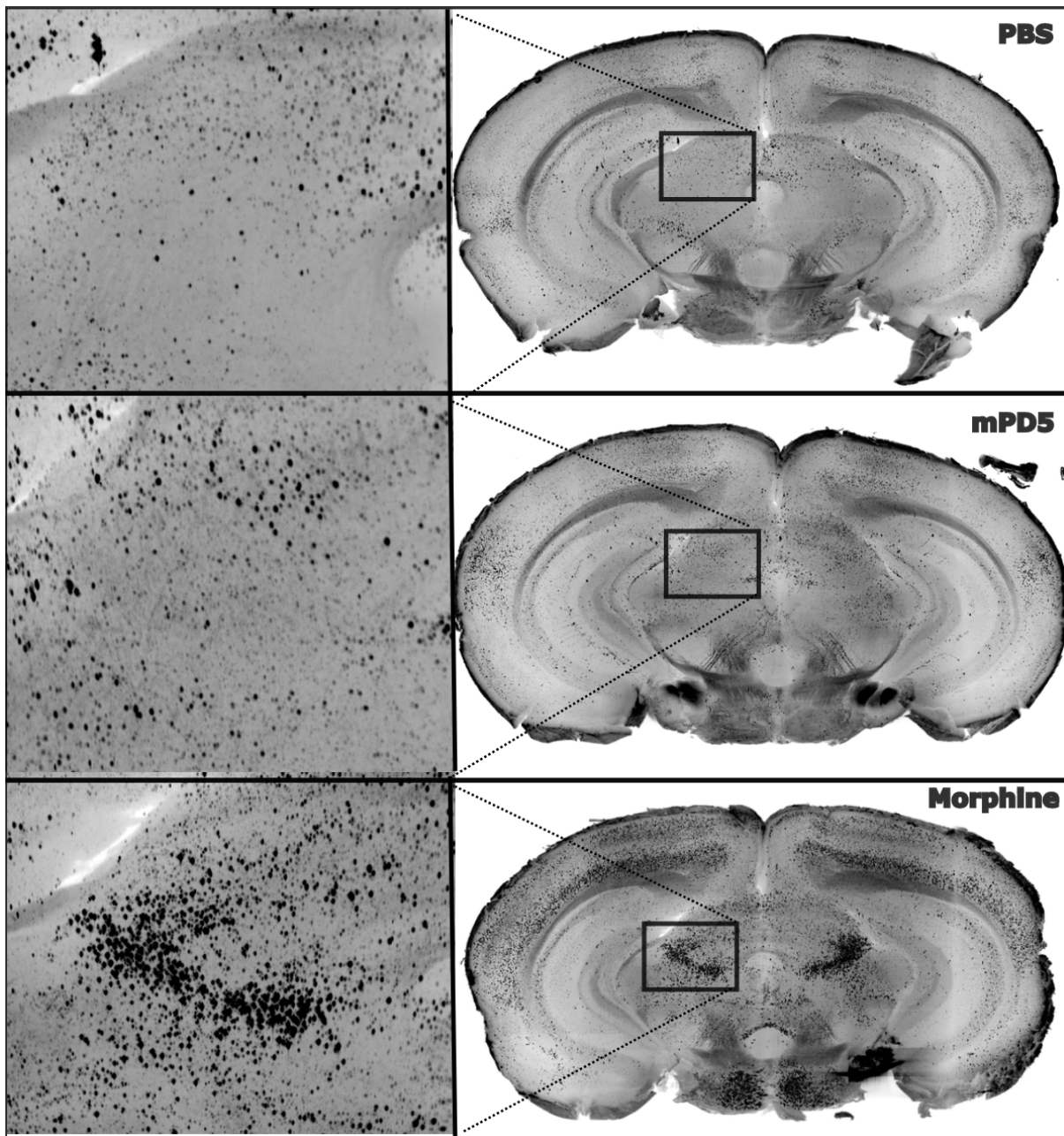


Figure 9. C-Fos expression in raw optical slices of a PBS, mPD5 and morphine brain.

Representative optical slices of 3 different SNI mice brains; PBS treated brain (A#11), mPD5 treated brain (C#35) and morphine treated brain (B#7). The optical sections of the coronal slices are 499 micrometers. The display settings are the same for all brains, min: 300, max: 1680, gamma: 1.

To explore if there were any significant differences in whole-brain total c-Fos positive cell counts between the three treatment groups (morphine, mPD5 and PBS), a Kruskal-Wallis followed by a Dunn's comparison was performed (*figure 10*). This test showed that morphine was statistically significantly different from both the mPD5-treated group ($p=0.0014$) and the PBS group ($p=0.007$) in the SNI cohort, (*figure 10A*), as well as statistically significantly different from the PBS ($p=0.0002$) and mPD5 ($p=0.023$) treated groups in the naive cohort, (*figure 10B*). No significant

difference in total c-Fos positive cell counts was detected between the mPD5 and PBS-treated groups, in either the SNI or naive cohorts, (*figure 10*).

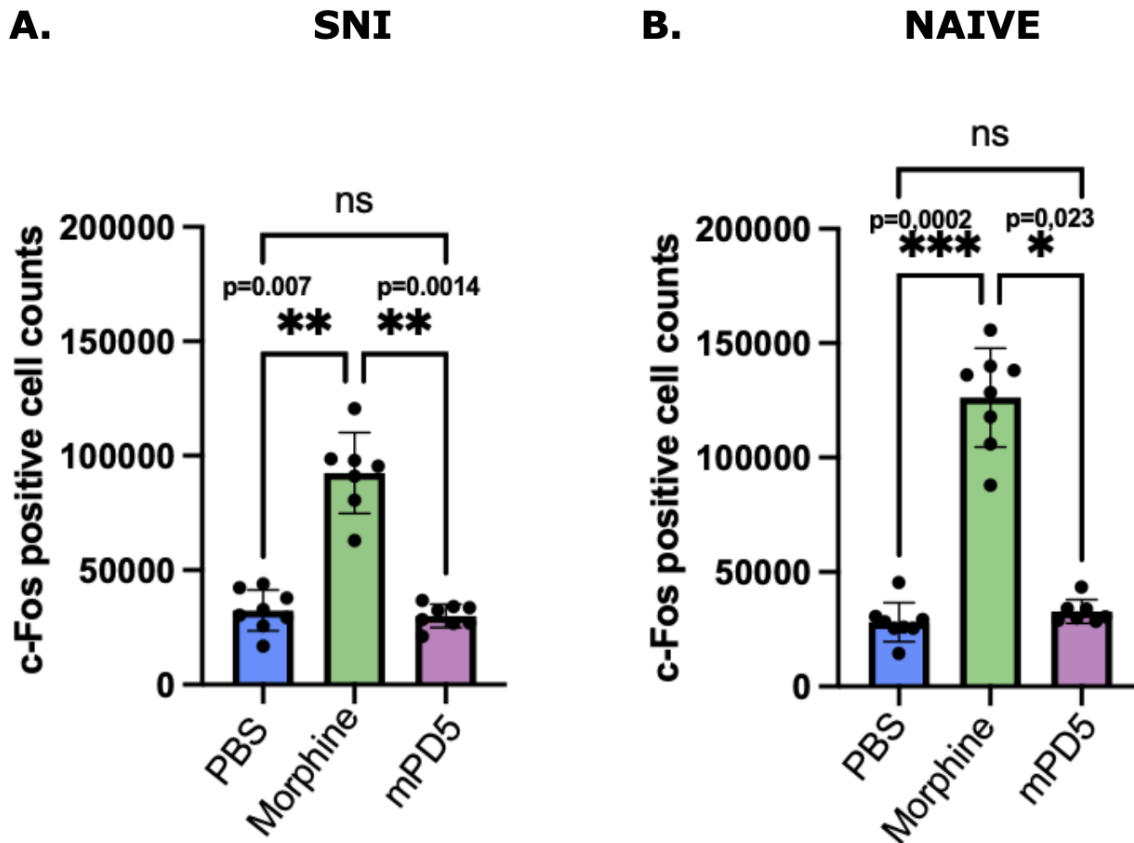


Figure 10. Statistical analysis of total c-Fos positive cell counts. Bar plot of whole-brain c-Fos positive cell counts in both the SNI cohort (A) and naive cohort (B).

The statistical analysis is a Kruskal-Wallis test followed by a Dunn's comparison test.

A. The SNI cohort morphine-treated mice are statistically significantly different from the mPD5 treated group, ($p=0.0014$)(**), and from the PBS group, ($p=0.007$)(**). The mPD5 treated group is not statistically significantly different from the PBS group (ns).

B. The naive cohort morphine treated mice are statistically significant different from the PBS treated group, ($p=0.0002$)(***) and from the mPD5 treated group ($p=0.023$)(*). The mPD5 treated group is not statistically significantly different from the PBS group (ns).

c-Fos expression changes in brain regions processing nociceptive information after mPD5 and morphine administration in the naive and SNI cohorts

Morphine vs PBS

To further understand how morphine affects the c-Fos expression at the brain region level, a comparison to the PBS group within the naive and SNI cohorts was performed using a Mann-Whitney U test. In the naive cohort, 467 brain regions had significantly ($p < 0.05$) more c-Fos positive cells in the morphine-treated group compared to the PBS group, (*figure 11A*). In the SNI cohort, 370 brain regions had significantly more c-Fos positive cells in the morphine-treated group compared to the PBS group, (*figure 11B*).

For both the naive and SNI cohorts, no brain regions were found with significantly fewer c-Fos positive cells in the morphine-treated group compared to the PBS group, (*figure 11*). The relative difference in cell counts between the morphine and PBS groups ranged up to a log₂ 8-fold change for the naive cohort and a log₂ 7-fold change for the SNI cohort, (*figure 11*).

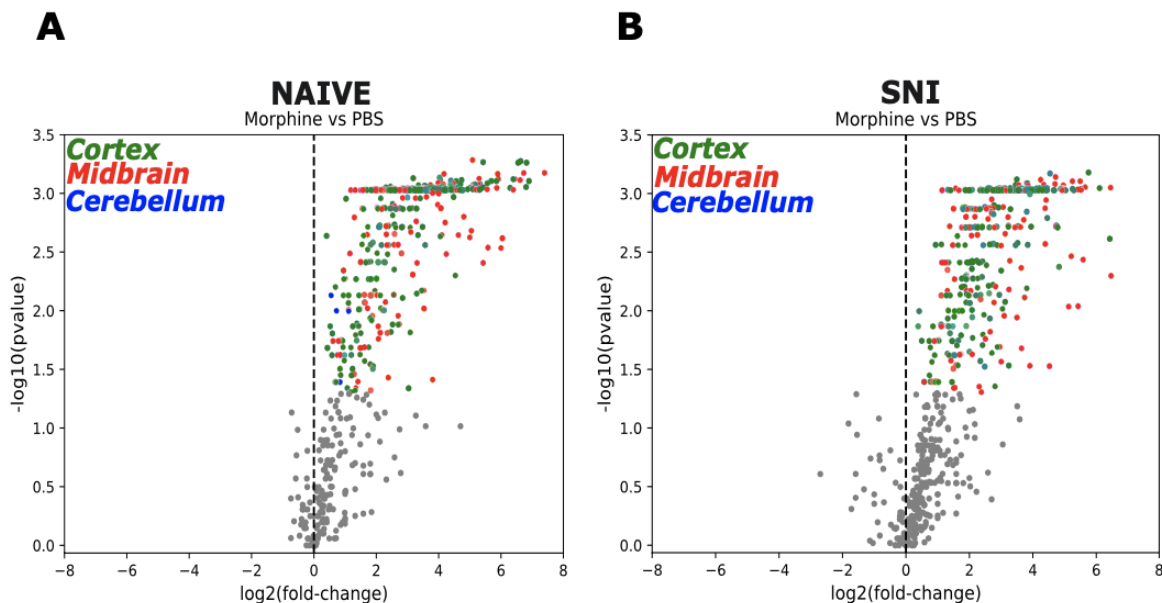


Figure 11. c-Fos brain region-wise comparison between morphine and PBS. Anatomically colored volcano plot of morphine vs PBS. A. Volcano Plot of morphine vs PBS in naive mice. B. Volcano Plot of morphine vs PBS in SNI mice. The significant regions are divided into three anatomical regions; cortex (green), midbrain (red) and cerebellum (blue). The volcano plot shows regions with significant increase (right) or decrease (left) in c-Fos positive cell counts in the morphine treated group compared to the PBS group. The x-axis represents the magnitude of difference of c-Fos positive cell counts from PBS to morphine. The y-axis represents the negative LogP-value. All dots represent a region of the mouse brain and the colored dots are the brain regions with significant ($p < 0.05$) change in the number of c-Fos positive cells.

To further assess how the c-Fos expression changes in brain regions processing nociceptive information following morphine administration, a comparison to the PBS group within the naive and SNI cohorts was performed using a Mann-Whitney U test. Morphine demonstrated significant ($p < 0.05$) c-Fos activity in 9-10 areas processing nociceptive information (S1, thalamus, RVM, medial prefrontal cortex (mPFC), AMG, ACC, Insula, PB, VTA and PAG) among many other regions in both the naive and SNI cohort, (*figure 12*). However, a few differences between the naive and SNI cohort were observed. The naive cohort had brain regions within the mPFC and ACC areas with significantly fewer c-Fos positive cells in the morphine-treated group compared to the PBS group than the SNI cohort had. This is evident, as the dark blue (mPFC) dots in the naive cohort were located at a log₂ 2-fold change, (*figure 12A*) whereas the dark-blue dots in the SNI cohort were located at a log₂ 5-fold change, (*figure 12B*). The same accounted for brain regions within the ACC where the burgundy dots in the naive cohort were located at a log₂ 1-fold change, (*figure 12A*), whereas the burgundy dots in the SNI cohort were located at a log₂ 4-fold change, (*figure 12B*). Among the brain regions with the highest significant ($p < 0.05$) difference in c-Fos positive cell counts for the SNI and naive morphine-treated mice compared to the PBS-treated mice was parapyramidal nucleus (PPY), which is a brain region in the RVM. Additionally, the VTA region displayed a 6.2-fold difference in c-Fos activity between the morphine-treated group and the PBS group, while the PL2/3 region displayed a 9.4-fold difference (see appendix 4 for fold-change calculations).

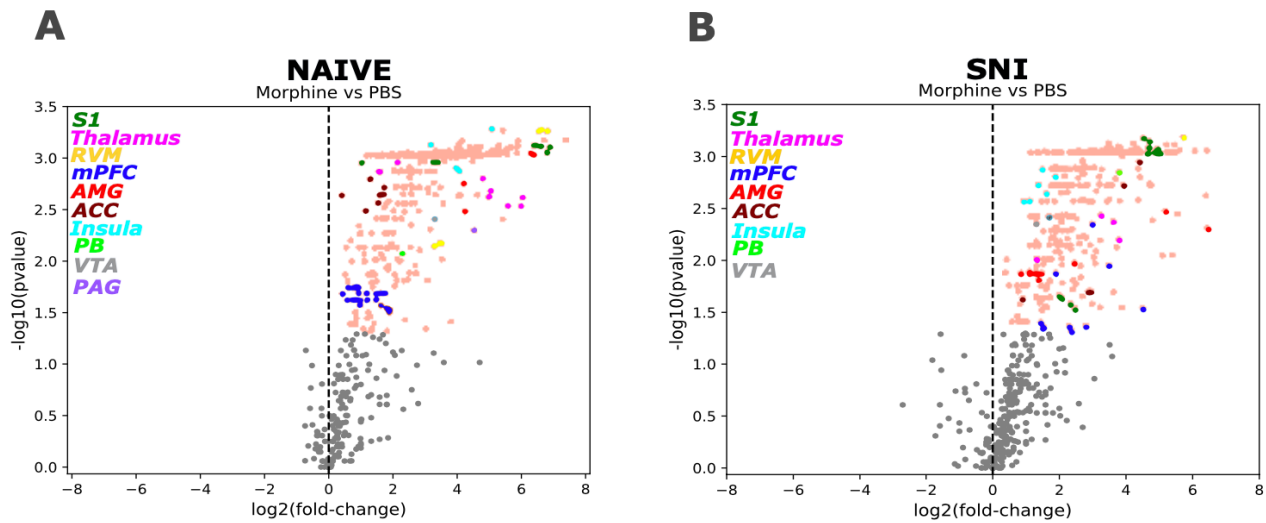


Figure 12. Brain region-wise comparison in regions processing nociceptive information between morphine and PBS. Anatomically colored volcano plot of morphine vs PBS. A. Volcano plot of morphine vs PBS in naive mice. B. Volcano plot of morphine vs PBS in SNI mice. The significant regions are divided into ten anatomical regions; S1 (green), thalamus (purple), RVM (orange), mPFC (blue), AMG (red), ACC (burgundy), insula (turquoise), PB (light-green), VTA (grey) and PAG (light-purple). The volcano plot shows regions with significant increase (right) or decrease (left) in c-Fos positive cell counts in the morphine treated group compared to the PBS group. The x-axis represents the magnitude of difference of c-Fos positive cell counts from PBS to morphine. The y-axis represents the negative LogP-value. All dots represent a region of the mouse brain and the colored dots are the brain regions with significant ($p < 0.05$) change in the number of c-Fos positive cells. S1: primary somatosensory cortex. RVM: rostral ventral medulla. mPFC: medial prefrontal cortex. AMG: amygdala. ACC: anterior cingulate cortex. PB: parabrachial nucleus. VTA: ventral tegmental area. PAG: periaqueductal grey.

To investigate the shared brain regions processing nociceptive information between the naive and SNI cohort following morphine administration, a Venn diagram was made. This resulted in 27 shared brain regions between the SNI and naive cohorts, (*figure 13*). These brain regions were located within the S1, thalamus, RVM, mPFC, AMG, ACC, Insula, PB, and VTA. For the naive cohort, 36 brain regions processing nociceptive information were detected within S1, thalamus, RVM, mPFC, AMG, ACC, Insula, PB, VTA, and PAG, while for the SNI cohort, 37 brain regions were detected within S1, thalamus, RVM, mPFC, AMG, ACC, Insula, PB, and VTA.

An interesting observation was that the naive morphine-treated cohort induced significant ($p < 0.05$) activity in the PAG, whereas the SNI morphine-treated cohort did not. Moreover, the SNI morphine-treated cohort had 4 additional S1 regions that were not shared with the naive cohort. These regions were primary somatosensory area, lower limb, layer 4 (SSp-ll4), primary somatosensory area, lower limb, layer 5 (ssp-ll5), primary somatosensory area, lower limb, layer

1(ssp-ll1) and primary somatosensory area, trunk, layer 4 (SSp-tr4), three of which are areas receiving information from the lower limb. The naive cohort had two regions within the thalamus, central lateral nucleus of the thalamus (CL), and interanterodorsal nucleus of the thalamus (IAD) which were not found with a significant ($p<0.05$) c-Fos positive cell count in the SNI cohort.

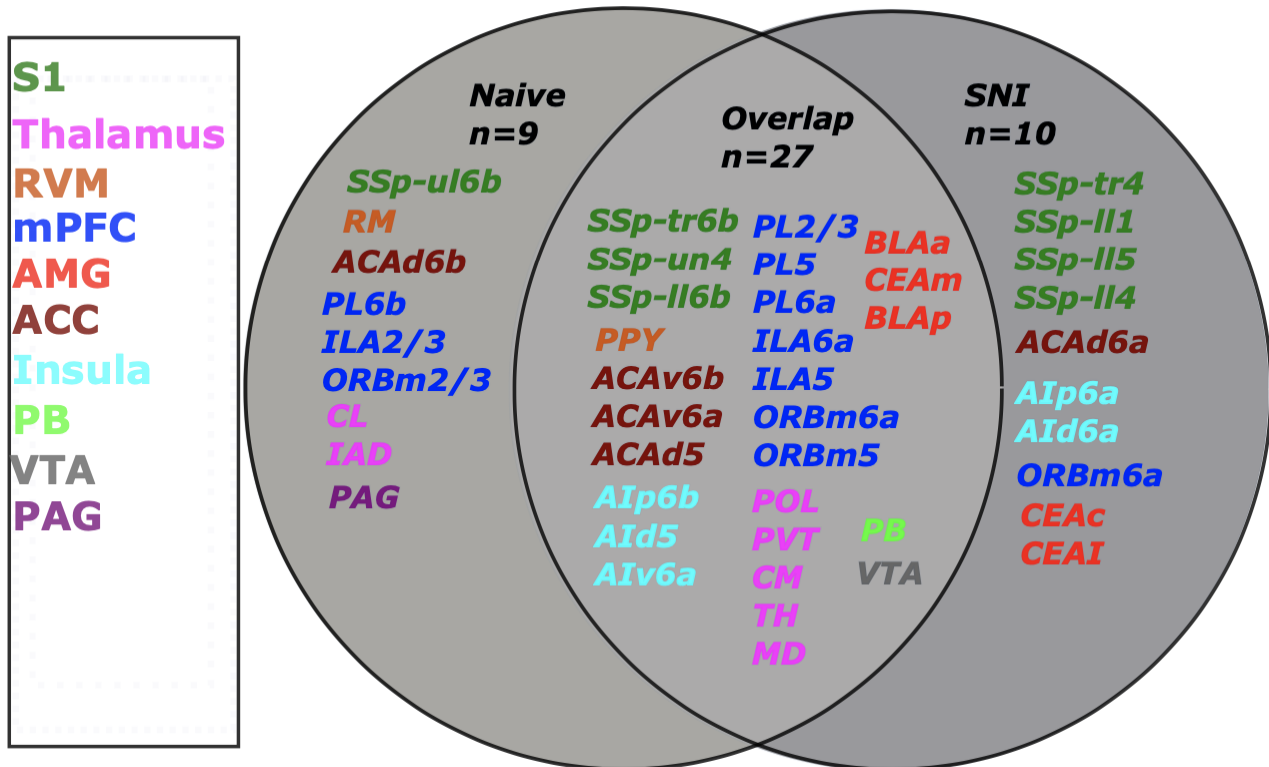


Figure 13. Shared brain regions, processing nociceptive information, between the naive and SNI cohort following morphine administration. Venn diagram illustrating color coded brain regions with significantly more c-Fos positive cells in the morphine-treated group compared to the PBS group for the SNI and naive cohort. The color coding is based on the brain regions processing nociceptive information: primary somatosensory cortex (S1, green), Thalamus (purple), rostral ventral medulla (RVM, orange), medial prefrontal cortex (mPFC, blue), amygdala (AMG, red), Anterior cingulate cortex (ACC, burgundy), insula (turquoise), Parabrachial nucleus (PB, light green), ventral tegmental area (VTA, grey) and periaqueductal grey (PAG, purple). The venn diagram is made in BioVenn.

The PAG brain region is involved in descending pain modulation and was not found with a significant ($p<0.05$) increase in c-Fos positive cells in the SNI mice following morphine administration. To confirm this, optical slices of raw SNI data for the PAG region in each individual PBS and morphine mouse brain were evaluated. Based on this, fewer c-Fos positive cells, represented as black dots, were found in the PAG region in the PBS mouse brains compared to the morphine mouse brains, (*figure 14*). Moreover, total c-Fos positive cell counts for the PAG region

varied within the PBS group, ranging from 207 to 1346 cells, and varied within the morphine group, ranging from 660 to 2258 cell counts, (figure 14).

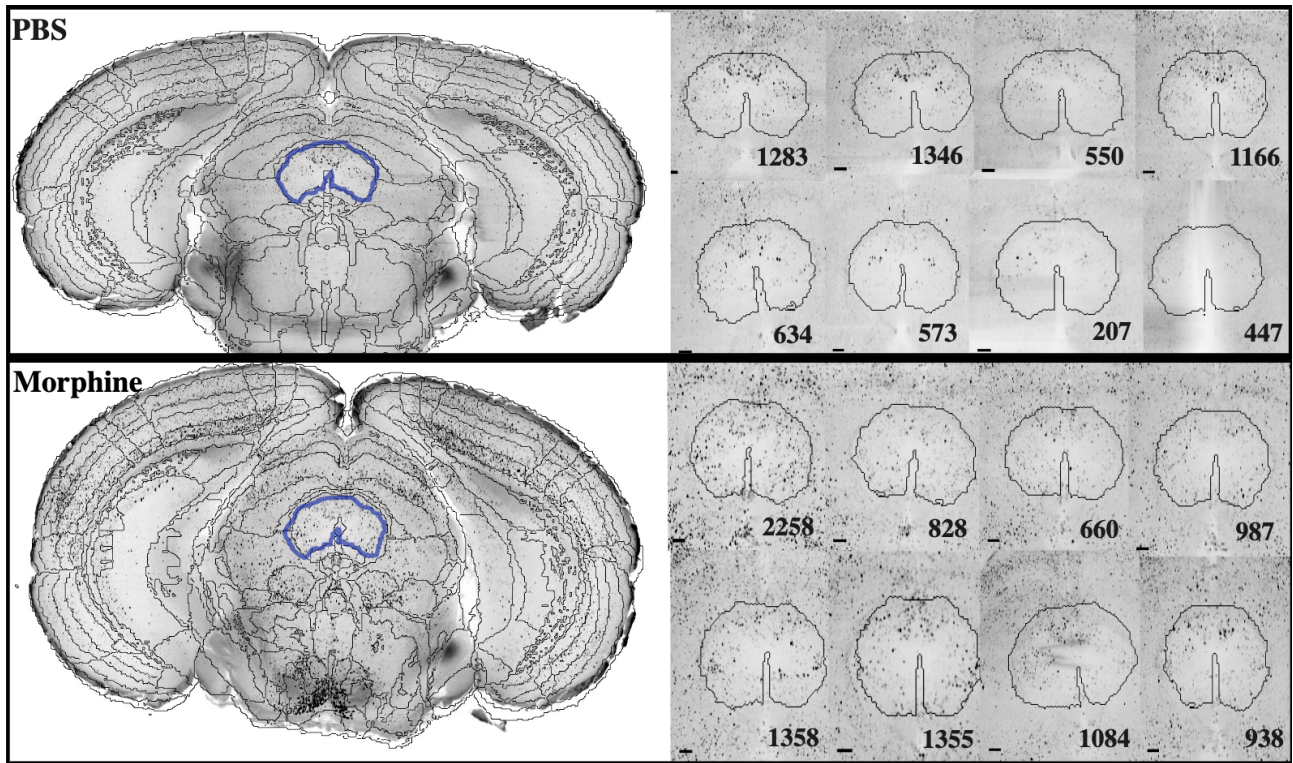


Figure 14. c-Fos expression in the PAG brain region in PBS and morphine brains. Optical slices of raw data from the SNI cohort. The PAG brain region is highlighted in blue. The PBS mice brains (n=8) are in the upper panel and the morphine brains (n=8) are in the lower panel. The c-Fos positive cell count for the entire PAG region is noted for every brain. The picture of each brain is represented by a single optical slice of 800 micrometers.

mPD5 vs PBS

To understand how mPD5 affects the c-Fos expression at the brain region level, a comparison to the PBS group within the naive and SNI cohorts was performed using on a Mann-Whitney U test. In the naive cohort, 39 brain regions had significantly ($p < 0.05$) more c-Fos positive cells in the mPD5-treated group compared to the PBS group, (figure 15A). Additionally, 3 brain regions had significantly fewer c-Fos positive cells in the mPD5 group compared to the PBS group, (figure 15A). In the SNI cohort, 8 brain regions had significantly ($p < 0.05$) more c-Fos positive cells in the mPD5-treated group compared to the PBS group, (figure 15B), and 6 brain regions had significantly fewer c-Fos positive cells in the mPD5 group compared to the PBS group, (figure 15B).

When comparing the SNI cohort to the naive cohort, most brain regions in the SNI cohort, such as SSp-II2/3, primary somatosensory area, undefined area, layer 1 (SSp-un1), primary somatosensory

area, mouth, layer 4 (SSp-m4), and posterior auditory area, layer 1 (AUDpo1) showed a log₂ 1-fold change in c-Fos positive cells in the mPD5 treated group compared to the PBS group. In the naive cohort, some brain regions had a log₂ fold change above 2, such as prelimbic area, layer 2/3 (PL2/3), tuberomamillary nucleus, dorsal part (TMd), visceral area, layer 2/3 (VISC2/3) and retrosplenial area, lateral agranular part, layer 6b (RSPagl6b). Notably, the SNI cohort showed most significant ($p < 0.05$) brain regions in cortical areas, whereas the naive cohort also showed significant ($p < 0.05$) brain regions in the midbrain and cerebellum. In the SNI cohort, only one brain region in the midbrain (TMd) had significantly ($p < 0.05$) more c-Fos positive cells in the mPD5 group compared to PBS. In contrast, 5 additional brain regions in the midbrain were found in the naive cohort: PB, CL, peripeduncular nucleus (PP), nucleus of reuniens (RE) and spinal nucleus of the trigeminal, caudal part (SPVC).

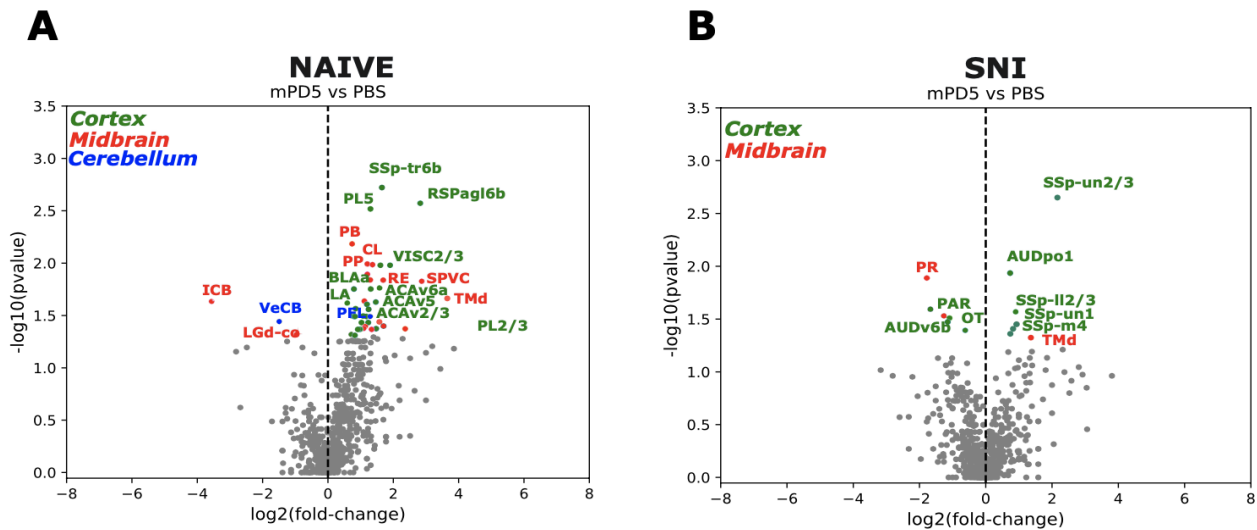


Figure 15. c-Fos brain region-wise comparison between mPD5 and PBS. Anatomically colored volcano plot of mPD5 vs PBS. A. Volcano plot of mPD5 vs PBS in naive mice. B. Volcano plot of mPD5 vs PBS in SNI mice. The significant regions are divided into three anatomical regions in the naive mice; cortex (green), midbrain (red) and cerebellum (blue), and two anatomical regions in SNI mice; cortex (green) and midbrain (red). The volcano plot shows regions with significant increase (right) or decrease (left) in c-Fos positive cell counts in the mPD5 treated group compared to the PBS group. The x-axis represents the magnitude of difference of c-Fos positive cell counts from PBS to mPD5. the y-axis represents the negative LogP-value. All dots represent a region of the mouse brain and the colored dots are the brain regions with significant ($p < 0.05$) change in the number of c-Fos positive cells.

To further assess how the c-Fos expression changes in brain regions processing nociceptive information following mPD5 administration, a comparison to the PBS group within the naive and SNI cohorts was performed using a Mann-Whitney U test. The naive mPD5 group demonstrated significant ($p < 0.05$) c-Fos activity in five brain areas processing nociceptive information (S1,

thalamus, mPFC, AMG, ACC, PB) among other regions, (*figure 16A*). The SNI mPD5 group demonstrated significant ($p < 0.05$) c-Fos activity in two brain areas processing nociceptive information (S1, thalamus) among others, (*figure 16B*).

The SNI mPD5 treated group, (*figure 16B*) demonstrated brain regions with significantly ($p < 0.05$) more c-Fos positive cells in the S1 area (primary somatosensory area, undefined area, layer 2/3 (SSp-un2/3), SSp-II2/3 and SSp-un1). No shared brain regions with significant ($p < 0.05$) c-Fos positive cell counts within the brain areas processing nociceptive information were detected between the naive and SNI cohorts.

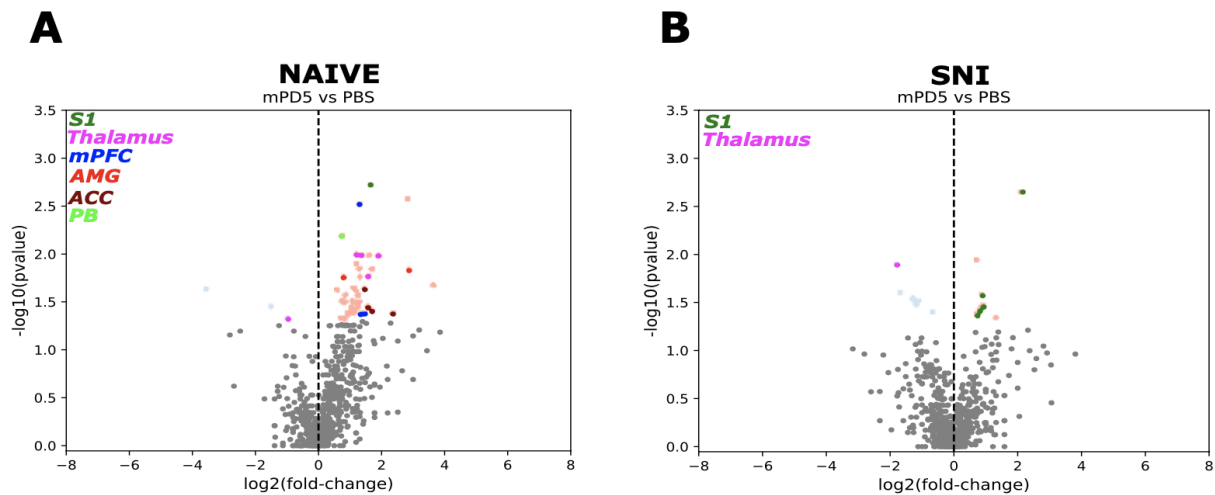


Figure 16. Brain region-wise comparison in regions processing nociceptive information between mPD5 and PBS. Anatomically colored volcano plot of mPD5 vs PBS. A. Volcano plot of mPD5 vs PBS in naive mice. B. Volcano plot of mPD5 vs PBS in SNI mice. The significant regions are divided into four anatomical regions for the naive; S1 (green), thalamus (purple), medial prefrontal cortex (mPFC, blue), amygdala (AMG, red) and anterior cingulate cortex (ACC, burgundy) and two anatomical regions for the SNI; primary somatosensory cortex (S1, green), thalamus (purple) and. The volcano plot shows regions with significant increase (right) or decrease (left) in c-Fos positive cell counts in the mPD5-treated group compared to the PBS group. The x-axis represents the magnitude of difference of c-Fos positive cell counts from PBS to mPD5. the y-axis represents the negative LogP-value. All dots represent a region of the mouse brain and the colored dots are the brain regions with significant ($p < 0.05$) change in the number of c-Fos positive cells.

The SSp-un2/3 region is part of the S1 area involved in processing nociceptive information and showed the highest fold change (log2 2-fold change) in cell counts between the mPD5 group and PBS group in the SNI cohort, (*figure 15B+16B*). To confirm this, optical slices of raw SNI data for the SSp-un2/3 region in each individual PBS and mPD5 mouse brain were evaluated.

No obvious change in the number of c-Fos positive cells, represented as black dots, was seen between the mPD5 treated group compared to the PBS group, (*figure 17*). When looking at the total c-Fos positive cell count in the whole SSp-un2/3 region for each brain, there were more c-Fos positive cells in the mPD5 mice than in the PBS mice. The total c-Fos positive cell count ranged from 5-24 cells in the mPD5 mice and from 0-8 cells in the PBS mice. It is noticeable that the alignment for the SSp-un2/3 region in one brain (mPD5 brain with 17 c-Fos positive cells) was off.

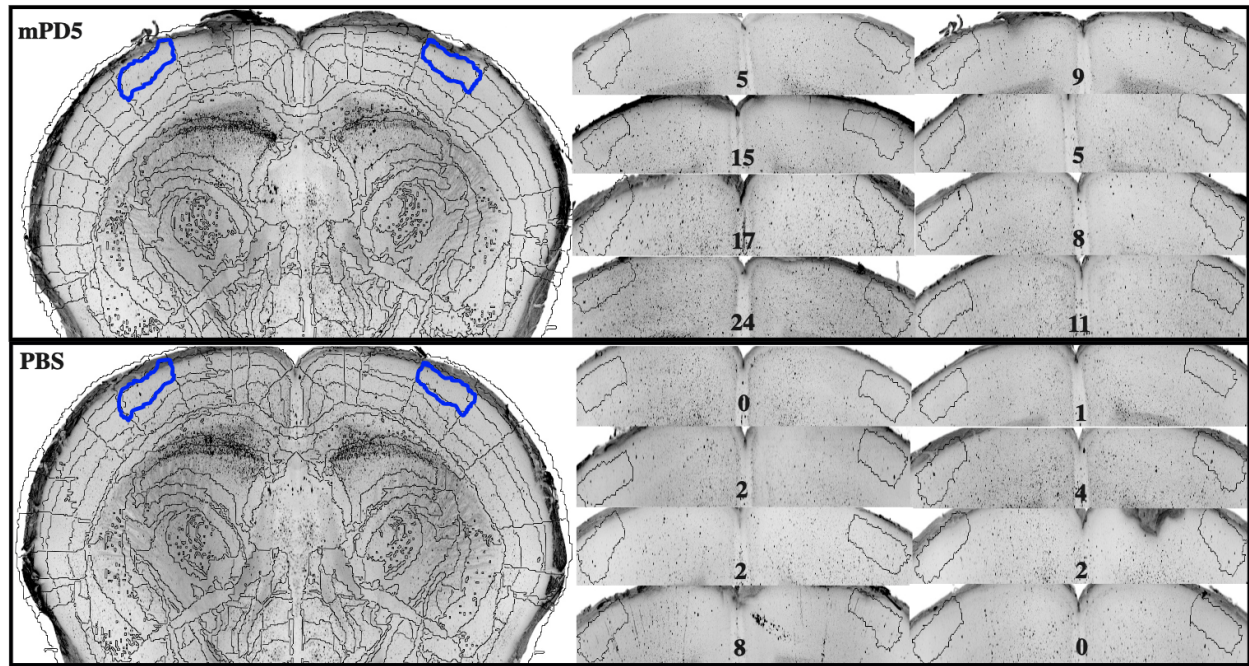


Figure 17. c-Fos expression in the SSp-un2/3 brain region in PBS and mPD5 brains. Optical slices of raw data from the SNI cohort. The SSp-un2/3 brain region is highlighted in blue and marked in the zoomed in view of each brain. The mPD5 mice brains (n=8) are in the upper panel and the PBS mice brains (n=8) are in the lower panel. The total c-Fos positive cell count for the SSp-un2/3 region is noted for every brain. The picture of each brain is represented by a single optical slice of 800 micrometers.

Unsuccessful staining with a pPDH antibody as a proxy for neuronal inhibition

To confirm the use of pPDH as a proxy for neuronal inhibition on a whole-brain scale, the staining protocol of the pPDH antibody was tested on 6 mice brains. The raw whole-brain images showed a halo appearing around all mice brains, (*figure 18*). Brain 4, 5, and 6 had the most visible halos. The brain with the least visible halo is brain 1, stained with the lowest antibody concentration (1:500) and had the longest incubation time of 14 days.

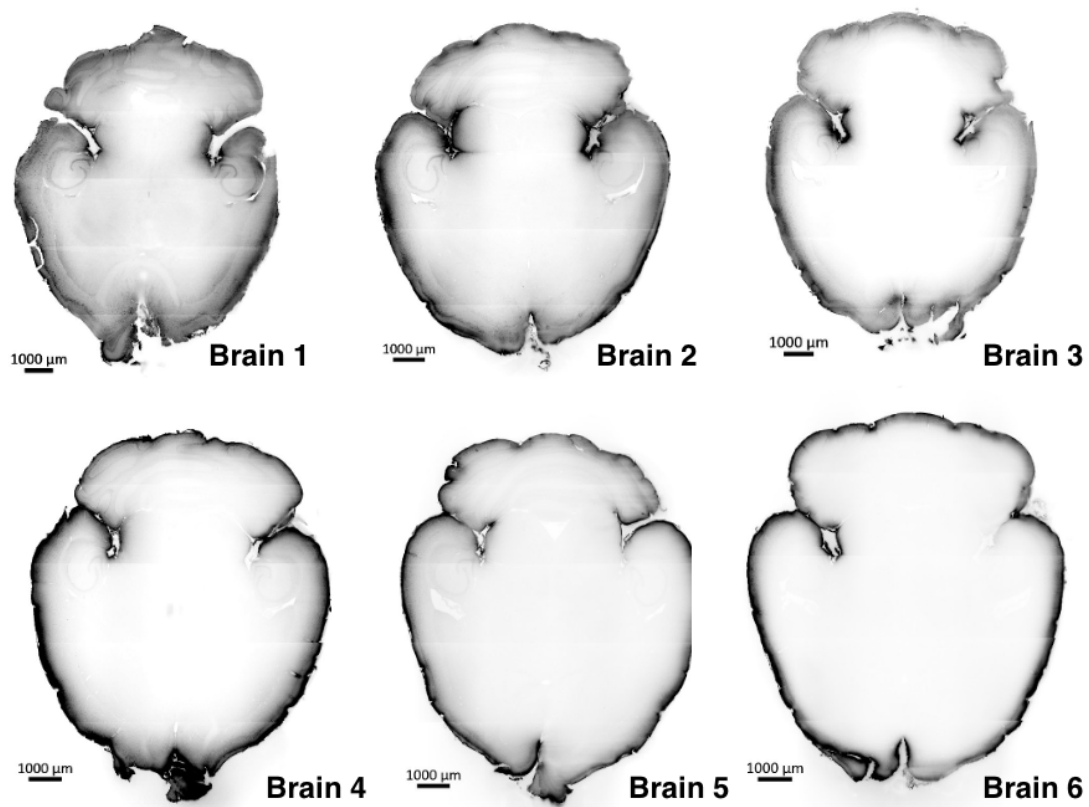


Figure 18. pPDH antibody staining. Illustration of raw whole-brain images generated from the Zeiss lightsheet 7 microscope of 6 mice stained with different concentrations of phosphorylated pyruvate dehydrogenase antibody at different incubation times. Brain 1 and 4 were incubated with 1:500 Phospho-Pyruvate Dehydrogenase $\alpha 1$ (Ser293) for 14 days. Brain 3 and 6 were incubated with 1:250 Phospho-Pyruvate Dehydrogenase $\alpha 1$ (Ser293) for 14 days. Brain 2 and 5 were incubated with 1:250 Phospho-Pyruvate Dehydrogenase $\alpha 1$ (Ser293) for 7 days. Images were acquired from ZEN 3.6 (blue edition) with the black and white dimensions: 58 and 27786 respectively. All images are acquired in the detection channel (CAM2).

Discussion

The aim of this study was firstly to investigate if there were any supraspinal changes in c-Fos expression in the SNI mice following the unilateral SNI surgery. No significant difference was detected in whole brain c-Fos positive cell counts between the non-treated SNI and naive mice, indicating that the SNI surgery did not cause c-Fos changes in the brain.

Moreover, this study aimed to confirm the widespread response of morphine in SNI and naive mice brains. In both the SNI and naive cohort, the morphine-treated group induced a widespread c-Fos expression in the brain.

Furthermore, this study aimed to see changes in c-Fos expression in brain regions processing nociceptive information, after morphine and mPD5 administration in both the naive and SNI cohort. Morphine induced increased c-Fos activity in 9-10 brain areas processing nociceptive information in both the SNI and naive cohort. On a whole brain level, the total c-Fos positive cell count showed no significant difference between the mPD5 and PBS group. However, the volcano plots showed some brain regions, processing nociceptive information, with an increase in activity in the mPD5-treated group compared to the PBS group.

Lastly, this study tested the staining protocol for pPDH as a proxy for neuronal inhibition on a whole-brain scale. However, the staining was not successful, as halos appearing around the brains could indicate insufficient penetration depth, a known challenge in 3D histology (Yau et al., 2023).

The supraspinal effects of the SNI model

This study did not observe a significant difference in the whole-brain total c-Fos positive cell counts between the non-treated SNI and naive mice. However, increased c-Fos activity was detected in specific brain regions of the naive mice, suggesting that the SNI model exerts a dampening effect on neuronal activity. Previous studies have reported increased c-Fos signals in the ACC following SNI surgery (Takeda et al., 2009; Tan et al., 2015), whereas the current study observed a general decrease in c-Fos signal post SNI surgery compared to the naive mice. Notably, Tan et al., (2015) reported increased c-Fos activity in the SNI mice after multiple noxious mechanical stimulations. In contrast, this study employed a single noxious mechanical stimulation on day 2 post SNI surgery, with SNI mice terminated and fixated on day 7 post SNI surgery. Therefore, it is questionable if the low c-Fos signal detected in the SNI mice in this study resulted from the limited number of noxious stimulations before fixation, given that c-Fos expression peaks 1-3 hours after stimulus and is transient. (Wu et al., 2006) Future studies could incorporate multiple mechanical noxious

stimulations of SNI mice at various time points prior to fixation, to obtain a more reliable c-Fos response correlating with evoked pain.

The SSp-II2/3 region, receiving nociceptive information from the lower limb, showed fewer c-Fos positive cells in the SNI group compared to the naive group. It is notable that decreased activity in this area was observed in the SNI mice, which is contrary to previous studies that demonstrated increased activity in the S1 region of chronic pain mice models (Chao et al., 2018; Hubbard et al., 2015; Kim et al., 2017). This discrepancy could be explained by the hypersensitivity of the affected area, leading mice to avoid putting pressure on it, as previously demonstrated by Mogil et al., (2010). This avoidance behavior could account for the reduced c-Fos positive cell count observed in the SSp-II2/3 region of the SNI cohort.

The analgesic effects of morphine and mPD5

Morphine

This study demonstrated that morphine administration caused a robust c-Fos expression in the brains of both the naive and SNI mice. As opioid receptors are expressed broadly throughout the entire brain, the widespread response is not surprising (Le Merrer et al., 2009). Previous studies have also reported increased c-Fos activity in various brain regions, including the limbic cortex, hypothalamus, midbrain and in some layers of the motor and somatosensory cortices following morphine administration in rats (Jerzemowska et al., 2022; Taracha et al., 2008). These findings are consistent with the increased c-Fos activity observed in the current study. Notably, morphine induced an increased c-Fos activity in 467 brain regions in naive mice and 370 brain regions in SNI mice out of 1290 regions analyzed. The significance of these regions was defined at a significance level of 0.05, and 261 of these brain regions had a significant c-Fos induction at a significance level of 0.001. This underscores the strong activity-inducing effects morphine has in the brain, as previously demonstrated (Jerzemowska et al., 2022; Taracha et al., 2008).

Morphine also increased the number of c-Fos positive cells in brain regions involved in nociceptive processing, such as RVM, AMG, ACC. These brain areas are all part of the descending modulation system, important for the facilitation and inhibition of pain. The induction of c-Fos in these areas following morphine administration has previously been reported in rats (Brynildsen et al., 2020; Jerzemowska et al., 2022).

However, it is worth mentioning that these regions represent only a minor fraction of the 467 brain regions with increased c-Fos positive cells in the morphine-treated group. This highlights that morphine activates a broad spectrum of brain regions beyond those involved in processing nociceptive information. Additionally, brain regions such as the VTA and PL2/3 showed increased c-Fos activity following morphine administration. Morphine-induced c-Fos activity has previously been found in VTA neurons, leading to the firing of dopamine neurons, contributing to the rewarding and addictive properties of morphine (Bontempi & Sharp, 1997). The PL2/3 region, part of the prelimbic cortex, is important for nociceptive and emotional modulation and neurons projecting from the prelimbic cortex to the AMG has displayed increased activity following SNI surgery (Gao et al., 2023). Based on the volcano plots, the VTA region showed a 6-fold difference in c-Fos activity between the morphine-treated group and the PBS group, while the PL2/3 region displayed a 9-fold difference. This finding is supportive of the known addictive properties and analgesic effects of morphine, as previously demonstrated by Bontempi & Sharp, (1997) and Gao et al., (2023). Brain region-wise comparison revealed that some brain regions with the most significant increase in c-Fos positive cells were located in the motor cortex, including MOs5, and Primary motor area, layer 6a (MOp6a) Secondary motor area, layer 6a (MOs6a). This finding aligns with a previous study using the same strain of mice as used for this study (C57BL/6), which reported strong increases in locomotion following morphine administration (Murphy et al., 2001).

Another noteworthy finding was the absence of increased c-Fos positive cells in the PAG region of the SNI cohort. The PAG region, involved in descending inhibitory control of nociception and rich in μ -opioid receptors, would be expected to show increased activity in the SNI cohort (Le Merrer et al., 2009). However, decreased activity in the PAG region following SNI surgery has previously been demonstrated using fMRI (Hubbard et al., 2015). Additionally, the c-Fos positive cells varied across brains within the morphine-treated group as well as within the PBS group of the SNI cohort, evident by the total c-Fos positive cell counts for the PAG region for each brain. This variability could be explained by biological variation, which has been demonstrated before by behavioral differences in an open-field test for the C57BL/6 strain of mice (Vidal, 2016). Such biological variation could reduce statistical power and render the PAG region non-significant in the SNI cohort, as no SNI mice in this study showed an increased c-Fos activity in the PAG region.

mPD5

mPD5 exert its effect by inhibiting PICK1, a protein highly conserved in the DRGs and layers I and II of the dorsal horn in the spinal cord (Sørensen et al., 2022). The localization of PICK1 in these regions is supported by Wang et al., (2011), who used PICK1 immunohistochemical staining to characterize the expression and distribution of PICK1 in the DRGs and in the dorsal horn of the spinal cord. However, the same study also highlighted the need for further exploration of PICK1 expression and distribution in pain-related regions of the nervous system (Wang et al., 2011). Thus, investigating the effect of mPD5 in the brain is relevant.

The current study found no significant difference in whole-brain total c-Fos positive cell count between the mPD5-treated group and the PBS group. However, at the brain region level, mPD5 induced an increase in c-Fos positive cell counts in 8 regions out of 1329, which is 362 fewer regions than morphine. The low detection of c-Fos in the mPD5-treated groups compared to morphine could indicate several things: mPD5 might not cross the blood-brain barrier, resulting in observed central responses due to peripheral effects; the c-Fos expression might be too small to detect following mPD5 administration; or c-Fos might be insufficient to demonstrate the effects of mPD5 in the brain. Lara Aparicio et al., (2022) stated that inhibited neurons will not express c-Fos, as c-Fos indicates cellular activity, limiting the study to excitatory pathways. Since mPD5 exerts its effect via inhibitory actions (Sørensen et al., 2022), co-staining the brains with an inhibitory antibody could provide better insight into mPD5's site of action. Additionally, the lack of effect in the brain supports the need for future studies to analyze the effect of mPD5 on c-Fos expression in the DRGs and dorsal horn of the spinal cord.

The analgesic effects of mPD5 have been demonstrated by relieving mechanical hyperalgesia (von Frey) and thermal hypersensitivity (Hargreaves) in a rodent model of neuropathic pain (Jensen et al., 2023; Sørensen et al., 2022). The volcano plots indicate that mPD5 activates regions within the S1 area, as regions within this area showed the greatest increase in c-Fos activity in the mPD5-treated groups. This finding is further supported by raw images, which show more c-Fos positive cells detected in the SSp-un2/3 region in the mPD5 mouse brain compared to PBS mouse brain. The involvement of S1 in the development of neuropathic pain has previously been found, with increased activity in the S1 region after SNI surgery in rats (Chao et al., 2018). The current study

detected an increased activity in this area following mPD5 administration in the SNI cohort, making the S1 area a target for further investigations to understand the modulatory actions of mPD5.

Another S1 region, the SSp-II2/3, showed more c-Fos positive cells in the mPD5-treated SNI cohort compared to the PBS group. As previously mentioned, the volcano plots showed fewer c-Fos positive cells in the SSp-II2/3 region in non-treated SNI mice, but the same region had more c-Fos positive cells in the SNI cohort following mPD5 administration. This could indicate that the mice no longer avoid putting pressure on the affected paw, suggesting that mPD5 provides pain relief.

Overall, the naive cohort showed more brain regions with an increased activity in the pain modulating areas than the SNI cohort after mPD5 administration. This could indicate that there are fewer sensitive brain regions in a neuropathic pain condition compared to a normal condition. Functional and structural changes following a peripheral induced injury have been found to increase activity in the thalamus and S1 region 4 weeks after SNI surgery in rats (Hubbard et al., 2015). The same study found increased activity in the ACC and prelimbic cortices 20 weeks after SNI surgery in rats, emphasizing that the structural changes in the brain post SNI surgery vary, with some activation patterns present after 4 weeks and others after 20 weeks (Hubbard et al., 2015). As the current study assessed c-Fos activity patterns 7 weeks post SNI surgery, it is questionable whether more time post-surgery would have changed the c-Fos activity seen in the mice brains. Moreover, KOVACS, (2008) states that c-Fos as a marker cannot distinguish between neurons activated by different stimuli. Based on this, it is likely that the detected c-Fos signal could be caused by other factors than mPD5, such as pain, light or sound, leading to false positives and making it difficult to detect a reliable signal from mPD5 in the SNI cohort.

A previous study examined the intrinsic rewarding characteristics of mPD5 using a single exposure place-preference experiment (Jensen et al., 2023), as initial sensitivity to the rewarding properties of drugs may play a crucial role as an endophenotype related to the susceptibility to addiction (Lambert et al., 2006). Jensen et al., (2023) found no abuse potential of mPD5 when compared to PBS in mice. Supporting this finding, the current study showed that mPD5 did not induce increased c-Fos activity in the VTA brain region, which is known to be implicated in addiction-associated behaviors (Brynildsen et al., 2020). Therefore, using mPD5 as an alternative to morphine for treating chronic neuropathic pain could be associated with a lower risk of abuse liability. However,

Jensen et al., (2023) mention that behavioral tests on full-scale conditioned place preference are necessary before making any definitive conclusions regarding addictive properties of mPD5 (Jensen et al., 2023).

Consideration for the employment of pPDH in future immunolabeling studies

Based on the raw whole-brain images of the neuronal inhibition marker pPDH, the labeling was found to be unsuccessful. One previous study by Yang, D. et al., (2023) successfully performed immunostaining on sections of mice brains using the pPDH monoclonal antibody. Although the current study employed the same pPDH antibody, the staining of whole mouse brains failed, as evidenced by halos appearing around all six mouse brains. Yang, D. et al., (2023) stained coronal sections of the mouse brain, whereas the current study performed staining on whole mice brains. This difference suggests that a larger antibody concentration of pPDH could potentially optimize the immunostaining. Alternatively, the halos in the raw images could indicate a lack of antibody penetration, which has previously been a challenge in mice brains, preventing staining of cells deeper than 100 micrometers (Sillitoe & Hawkes, 2002). In summary, future studies should optimize the tissue clearing protocol for immunostaining with pPDH to enhance antibody penetration for effective whole-brain immunostaining.

Limitations

In general, the naive cohort had more c-Fos activity than the SNI cohort. It is worth mentioning that the SNI and naive cohorts have been handled the same way, but they have not been handled the same day, which could result in cohort variability, making it difficult to compare the two cohorts. Moreover, the handling of the two cohorts at different days could allow for other factors to influence the c-Fos induction, than the treatments. The expression of c-Fos has previously been studied in relation to different stressors, where one study found increases in c-Fos expression in rats following exposure to high sound (Svendsen & Lykkegaard, 2001), another study found that both the handling and the use of anesthetics increased the cerebral c-Fos induction in rats (Asanuma & Ogawa, 1994). This emphasizes that c-Fos is a sensitive marker for neuronal activity, which could make it difficult to compare across different cohorts.

This study demonstrated that mPD5 induced c-Fos expression in brain regions that process nociceptive information. The induction of c-Fos is widely used and accepted as a marker for neuronal activation, and its increased expression in areas associated with pain processing supports

the hypothesis that mPD5 may modulate pain perception pathways. However, the translation of analgesic efficacy from rodent models to human clinical settings remains challenging. Eisenach & Rice, (2022) have highlighted, the success rate of preclinical research in predicting clinical efficacy as poor and believes that it is often attributed to methodological flaws in rodent studies, which can lead to the identification and validation of targets that do not translate well to humans. The complexity of pain mechanisms and the differences between rodent and human physiology contribute to these translational challenges (Eisenach & Rice, 2022). Despite these challenges, the use of rodent models in testing drug efficacy is approved by the NIH. The NIH emphasizes the importance of high throughput screening of novel analgesics in rodent models before processing to further testing stages. (Domínguez-Olivía Adriana et al., 2023) While mPD5 shows promising analgesic effects based on its ability to induce c-Fos expression in pain modulating areas in rodents, further research is necessary to validate these findings in human studies. Improving methods of rodent studies and developing better translational models will be crucial in enhancing the predictive value of preclinical research to clinical outcomes.

Conclusion

In conclusion, no difference in whole-brain c-Fos positive cell counts were detected between non-treated SNI and naive, suggesting that SNI surgery did not cause widespread c-Fos changes in the brain. Morphine administration induced a robust and widespread c-Fos response in both the SNI and naive mice, highlighting its potent activity-inducing effects on the brain. Morphine increased c-Fos activity in several brain regions involved in pain modulation, including RVM, AMG and ACC. In contrast, mPD5 treatment resulted in fewer brain regions with increased c-Fos activity compared to morphine, suggesting that mPD5 does not directly affect the brain. The mPD5-treated SNI cohort showed increased c-Fos activity in specific somatosensory areas implicated in processing of nociceptive information.

Additionally, the study tested the staining protocol for pPDH as a proxy for neuronal inhibition on a whole-brain scale. However, the staining was not successful, indicating a need for protocol optimization.

Overall, the findings suggest that while morphine has widespread effects on brain activity, mPD5 may offer a more selective therapeutic approach for neuropathic pain with potentially fewer side effects related to addiction.

References

- Alok, K. P. (2021). Profiling the Effects of Repetitive Morphine Administration on Motor Behavior in Rats. <https://www.ncbi.nlm.nih.gov/pmc/articles/PMC8308092/>
doi: 10.3390/molecules26144355
- Apkarian, A. V., Bushnell, M. C., Treede, R., & Zubieta, J. (2005). Human brain mechanisms of pain perception and regulation in health and disease. *European Journal of Pain*, 9(4), 463.
<https://pubmed.ncbi.nlm.nih.gov/15979027/> 10.1016/j.ejpain.2004.11.001
- Arendt-Nielsen, L., Skou, S. T., Nielsen, T. A., & Petersen, K. K. (2015). Altered Central Sensitization and Pain Modulation in the CNS in Chronic Joint Pain. *Current Osteoporosis Reports*, 13(4), 225-234. <https://pubmed.ncbi.nlm.nih.gov/26026770/> 10.1007/s11914-015-0276-x
- Asanuma, M., & Ogawa, N. (1994). Pitfalls in Assessment of c-fos mRNA Expression in the Brain: Effects of Animal Handling. *Reviews in the Neurosciences*, 5(2), 171-178.
<https://pubmed.ncbi.nlm.nih.gov/7827709/> 10.1515/REVNEURO.1994.5.2.171
- Atianjoh, F. E., Yaster, M., Zhao, X., Takamiya, K., Xia, J., Gauda, E. B., Huganir, R. L., & Tao, Y. (2010). Spinal cord protein interacting with C kinase 1 is required for the maintenance of complete Freund's adjuvant-induced inflammatory pain but not for incision-induced post-operative pain. *Pain (Amsterdam)*, 151(1), 226-234.
<https://pubmed.ncbi.nlm.nih.gov/20696523/> 10.1016/j.pain.2010.07.017

- Bontempi, B., & Sharp, F. R. (1997). Systemic Morphine-Induced Fos Protein in the Rat Striatum and Nucleus Accumbens Is Regulated by μ Opioid Receptors in the Substantia Nigra and Ventral Tegmental Area. *The Journal of Neuroscience*, 17(21), 8596-8612.
<https://pubmed.ncbi.nlm.nih.gov/9334431/> 10.1523/jneurosci.17-21-08596.1997
- Bria, A., & Iannello, G. (2012). TeraStitcher - A tool for fast automatic 3D-stitching of teravoxel-sized microscopy images. *BMC Bioinformatics*, 13(1), 316-316.
<https://pubmed.ncbi.nlm.nih.gov/23181553/> 10.1186/1471-2105-13-316
- Brynildsen, J. K., Mace, K. D., Cornblath, E. J., Weidler, C., Pasqualetti, F., Bassett, D. S., & Blendy, J. A. (2020). Gene coexpression patterns predict opiate-induced brain-state transitions. *Proceedings of the National Academy of Sciences - PNAS*, 117(32), 19556-19565.
<https://pubmed.ncbi.nlm.nih.gov/32694207/> 10.1073/pnas.2003601117
- Chao, T. H., Chen, J., & Yen, C. (2018). Plasticity changes in forebrain activity and functional connectivity during neuropathic pain development in rats with sciatic spared nerve injury. *Molecular Brain*, 11(1), 55. <https://pubmed.ncbi.nlm.nih.gov/30285801/> 10.1186/s13041-018-0398-z
- Chen, M., Zhao, Y., Yang, H., Luan, W., Song, J., Cui, D., Dong, Y., Lai, B., Ma, L., & Zheng, P. (2015). Morphine disinhibits glutamatergic input to VTA dopamine neurons and promotes dopamine neuron excitation. *eLife*, <https://www.ncbi.nlm.nih.gov/pmc/articles/PMC4538365/> 410.7554/eLife.09275
- Christensen, N. R., De Luca, M., Lever, M. B., Richner, M., Hansen, A. B., Noes-Holt, G., Jensen, K. L., Rathje, M., Jensen, D. B., Erlendsson, S., Bartling, C. R., Ammendrup-Johnsen, I., Pedersen, S. E., Schönauer, M., Nissen, K. B., Midtgaard, S. R., Teilum, K., Arleth, L.,

Sørensen, A. T., . . . Madsen, K. L. (2020). A high-affinity, bivalent PDZ domain inhibitor complexes PICK1 to alleviate neuropathic pain. *EMBO Molecular Medicine*, 12(6), e11248-n/a. <https://pubmed.ncbi.nlm.nih.gov/32352640/> 10.15252/emmm.201911248

Cichon, J., Sun, L., & Yang, G. (2018). Spared Nerve Injury Model of Neuropathic Pain in Mice. *Bio-Protocol*, 8(6), e2777. <https://www.ncbi.nlm.nih.gov/pmc/articles/PMC5906065/> 10.21769/bioprotoc.2777

Cohen, S. P., & Mao, J. (2014). Neuropathic pain: mechanisms and their clinical implications. *BMJ (Online)*, 348(feb05 6), f7656. <https://pubmed.ncbi.nlm.nih.gov/24500412/> 10.1136/bmj.f7656

Cooper, T. E., Chen, J., Wiffen, P. J., Derry, S., Carr, D. B., Aldington, D., Cole, P., Moore, R. A., & Wiffen, P. J. (2017). Morphine for chronic neuropathic pain in adults. *Cochrane Database of Systematic Reviews*, 2019(5), CD011669. <https://www.ncbi.nlm.nih.gov/pmc/articles/PMC6481499/> 10.1002/14651858.cd011669.pub2

COSTIGAN, M., SCHOLZ, J., & WOOLF, C. J. (2009). Neuropathic Pain: A Maladaptive Response of the Nervous System to Damage. *Annual Review of Neuroscience*, 32(1), 1-32. <https://pubmed.ncbi.nlm.nih.gov/19400724/> 10.1146/annurev.neuro.051508.135531

Cull-Candy, S. G., & Farrant, M. (2021). Ca²⁺-permeable AMPA receptors and their auxiliary subunits in synaptic plasticity and disease. *The Journal of Physiology*, 599(10), 2655-2671. <https://pubmed.ncbi.nlm.nih.gov/33533533/> 10.1113/JP279029

Domínguez-Olivia Adriana et al. (2023). The Importance of Animal Models in Biomedical Research: Current Insights and Applications. <https://pubmed.ncbi.nlm.nih.gov/37048478/> DOI: 10.3390/ani13071223

Duraku, L. S., Hossaini, M., Hoendervangers, S., Falke, L. L., Kambiz, S., Mudera, V. C., Holstege, J. C., Walbeehm, E. T., & Ruigrok, T. J. H. (2012). Spatiotemporal Dynamics of Re-Innervation and Hyperinnervation Patterns by Uninjured CGRP Fibers in the Rat Foot Sole Epidermis after Nerve Injury. *Molecular Pain*, 8(1), 61.

<https://pubmed.ncbi.nlm.nih.gov/22935198/> 10.1186/1744-8069-8-61

Eisenach, J. C., & Rice, A. S. C. (2022). Improving Preclinical Development of Novel Interventions to Treat Pain: Insanity Is Doing the Same Thing Over and Over and Expecting Different Results. *Anesthesia and Analgesia*, 135(6), 1128-1136.

<https://pubmed.ncbi.nlm.nih.gov/36384008/> 10.1213/ANE.00000000000006249

Fadahunsi, N., Petersen, J., Metz, S., Jakobsen, A., Vad Mathiesen, C., Silke Buch-Rasmussen, A., Kurgan, N., Kjærgaard Larsen, J., Andersen, R. C., Topilko, T., Svendsen, C., Apuschkin, M., Skovbjerg, G., Hendrik Schmidt, J., Houser, G., Elgaard Jager, S., Bach, A., Deshmukh, A. S., Kilpeläinen, T. O., . . . Clemmensen, C. (2024). Targeting postsynaptic glutamate receptor scaffolding proteins PSD-95 and PICK1 for obesity treatment. *Science Advances*, 10(9), eadg2636. <https://www.science.org/doi/10.1126/sciadv.adg2636> 10.1126/sciadv.adg2636

Finnerup, N. B., Haroutounian, S., Baron, R., Dworkin, R. H., Gilron, I., Haanpaa, M., Jensen, T. S., Kamerman, P. R., McNicol, E., Moore, A., Raja, S. N., Andersen, N. T., Sena, E. S., Smith, B. H., Rice, A. S. C., & Attal, N. (2018). Neuropathic pain clinical trials: factors associated with decreases in estimated drug efficacy. *Pain (Amsterdam)*, 159(11), 2339-2346.

<https://pubmed.ncbi.nlm.nih.gov/30015707/> 10.1097/j.pain.0000000000001340

- Gao, F., Huang, J., Huang, G., You, Q., Yao, S., Zhao, S., Liu, J., Wu, C., Chen, G., Liu, S., Yu, Z., Zhou, Y., Ning, Y., Liu, S., Hu, B., & Sun, X. (2023). Elevated prelimbic cortex-to-basolateral amygdala circuit activity mediates comorbid anxiety-like behaviors associated with chronic pain. *The Journal of Clinical Investigation*, 133(9) <https://pubmed.ncbi.nlm.nih.gov/36917193/> 10.1172/JCI166356
- Geuter, S., Reynolds Losin, E. A., Roy, M., Atlas, L. Y., Schmidt, L., Krishnan, A., Koban, L., Wager, T. D., & Lindquist, M. A. (2020). Multiple Brain Networks Mediating Stimulus–Pain Relationships in Humans. *Cerebral Cortex*, 30(7), 4204-4219. <https://pubmed.ncbi.nlm.nih.gov/32219311/> 10.1093/cercor/bhaa048
- Glick, S., Sotocinal, S. G., Chanda, M. L., Echols, S., Bailey, A. L., Wong, D., Mogil, J. S., Matsumiya, L., LaCroix-Fralish, M. L., van den Maagdenberg, Arn M J M, Ferrari, M. D., Klassen-Ross, T., Clarke, S. E., Craig, K. D., Drummond, T. E., Sorge, R. E., Tabaka, J. M., Langford, D. J., & Ingrao, J. (2010). Coding of facial expressions of pain in the laboratory mouse. *Nature Methods*, 7(6), 447-449. <https://www.nature.com/articles/nmeth.1455> 10.1038/nmeth.1455
- Guida, F., De Gregorio, D., Palazzo, E., Ricciardi, F., Boccella, S., Belardo, C., Iannotta, M., Infantino, R., Formato, F., Marabese, I., Luongo, L., de Novellis, V., & Maione, S. (2020). Behavioral, Biochemical and Electrophysiological Changes in Spared Nerve Injury Model of Neuropathic Pain. *International Journal of Molecular Sciences*, 21(9), 3396. <https://www.ncbi.nlm.nih.gov/pmc/articles/PMC7246983/> 10.3390/ijms21093396
- Hossaini, M., Duraku, L. S., Kohli, S. K., Jongen, J. L. M., & Holstege, J. C. (2014). Spinal distribution of c-Fos activated neurons expressing enkephalin in acute and chronic pain

models. *Brain Research*, 1543, 83-92. <https://pubmed.ncbi.nlm.nih.gov/24231552/>
10.1016/j.brainres.2013.10.044

Hubbard, C. S., Khan, S. A., Xu, S., Cha, M., Masri, R., & Seminowicz, D. A. (2015). Behavioral, metabolic and functional brain changes in a rat model of chronic neuropathic pain: A longitudinal MRI study. *NeuroImage*, 107, 333-344.

<https://pubmed.ncbi.nlm.nih.gov/25524649/> 10.1016/j.neuroimage.2014.12.024

Jensen et al., Christensen, N., Noes-Holt, G., Kannevorf, I., Sivertsen, L., Baro, R., Fernández, L., Goddard, C., Hopkins, C., Thomsen, C., Soltan, I., Castillo, M., Jager, S., Tidemand, F., Arleth, L., Hedegaard, A., Sørensen, A., Madsen, K., (2023). mPD5, an efficacious PICK1 inhibitor for treating chronic pain. *Health & Medicine Week*,

<https://www.biorxiv.org/content/10.1101/2023.03.03.530471v1>, 7509.

Jerzemowska, G., Plucińska, K., Piwka, A., Podlacha, M., & Orzeł-Gryglewska, J. (2022).

Behavioral Reaction and c-fos Expression after Opioids Injection into the Pedunculopontine Tegmental Nucleus and Electrical Stimulation of the Ventral Tegmental Area. *International Journal of Molecular Sciences*, 24(1), 512. <https://pubmed.ncbi.nlm.nih.gov/36613953/>
m10.3390/ijms24010512

Kang, Y., Trewern, L., Jackman, J., McCartney, D., & Soni, A. (2023). Chronic pain: definitions and diagnosis. *BMJ (Online)*, 381, e076036. <https://www.bmj.com/content/381/bmj-2023-076036> 10.1136/bmj-2023-076036

Kim, W., Kim, S. K., & Nabekura, J. (2017). Functional and structural plasticity in the primary somatosensory cortex associated with chronic pain. *Journal of Neurochemistry*, 141(4), 499-506. <https://pubmed.ncbi.nlm.nih.gov/28278355/> 10.1111/jnc.14012

- Kopach, O., Kao, S., Petralia, R. S., Belan, P., Tao, Y., & Voitenko, N. (2011). Inflammation alters trafficking of extrasynaptic AMPA receptors in tonically firing lamina II neurons of the rat spinal dorsal horn. *Pain*, 152(4), 912-923. <https://pubmed.ncbi.nlm.nih.gov/21282008/> 10.1016/j.pain.2011.01.016
- KOVACS, K. J. (2008). Measurement of Immediate-Early Gene Activation- c-fos and Beyond. *Journal of Neuroendocrinology*, 20(6), 665-672. <https://onlinelibrary.wiley.com/doi/full/10.1111/j.1365-2826.2008.01734.x> 10.1111/j.1365-2826.2008.01734.x
- Lambert, N. M., McLeod, M., & Schenk, S. (2006). Subjective responses to initial experience with cocaine: an exploration of the incentive-sensitization theory of drug abuse. *Addiction (Abingdon, England)*, 101(5), 713-725. <https://pubmed.ncbi.nlm.nih.gov/16669905/> 10.1111/j.1360-0443.2006.01408.x
- Lara Aparicio, S. Y., Laureani Fierro, Á d. J., Aranda Abreu, G. E., Toledo Cárdenas, R., García Hernández, L. I., Coria Ávila, G. A., Rojas Durán, F., Aguilar, M. E. H., Manzo Denes, J., Chi-Castañeda, L. D., & Pérez Estudillo, C. A. (2022). Current Opinion on the Use of c-Fos in Neuroscience. *NeuroSci*, 3(4), 687-702. <https://www.mdpi.com/2673-4087/3/4/50> 10.3390/neurosci3040050
- Latremoliere, A., & Woolf, C. J. (2009). Central Sensitization: A Generator of Pain Hypersensitivity by Central Neural Plasticity. *The Journal of Pain*, 10(9), 895-926. <https://www.ncbi.nlm.nih.gov/pmc/articles/PMC2750819/> 10.1016/j.jpain.2009.06.012
- Lazzarino, G., Amorini, A. M., Signoretti, S., Musumeci, G., Lazzarino, G., Caruso, G., Pastore, F. S., Di Pietro, V., Tavazzi, B., & Belli, A. (2019). Pyruvate Dehydrogenase and Tricarboxylic

Acid Cycle Enzymes Are Sensitive Targets of Traumatic Brain Injury Induced Metabolic Derangement. *International Journal of Molecular Sciences*, 20(22), 5774.

<https://pubmed.ncbi.nlm.nih.gov/31744143/> 10.3390/ijms20225774

Le Merrer, J., Becker, J. A. J., Befort, K., & Kieffer, B. L. (2009). Reward Processing by the Opioid System in the Brain. *Physiological Reviews*, 89(4), 1379-1412.

<https://www.ncbi.nlm.nih.gov/pmc/articles/PMC4482114/> 10.1152/physrev.00005.2009

Legrain, V., Iannetti, G. D., Plaghki, L., & Mouraux, A. (2011). The pain matrix reloaded: a salience detection system for the body. *Progress in Neurobiology*, 93(1), 111-124.

<https://pubmed.ncbi.nlm.nih.gov/21040755/> 10.1016/j.pneurobio.2010.10.005

Lindquist, M. A., Krishnan, A., López-Solà, M., Jepma, M., Woo, C., Koban, L., Roy, M., Atlas, L. Y., Schmidt, L., Chang, L. J., Reynolds Losin, E. A., Eisenbarth, H., Ashar, Y. K., Delk, E., & Wager, T. D. (2017). Group-regularized individual prediction: theory and application to pain. *NeuroImage (Orlando, Fla.)*, 145(Pt B), 274-287. <https://pubmed.ncbi.nlm.nih.gov/26592808/> 10.1016/j.neuroimage.2015.10.074

Listos, J., Łupina, M., Talarek, S., Mazur, A., Orzelska-Górka, J., & Kotlińska, J. (2019). The Mechanisms Involved in Morphine Addiction: An Overview. *International Journal of*

Molecular Sciences, 20(17), 4302. <https://www.ncbi.nlm.nih.gov/pmc/articles/PMC6747116/> 10.3390/ijms20174302

Mogil, J. S., Graham, A. C., Ritchie, J., Hughes, S. F., Austin, J., Schorscher-Petcu, A., Langford, D. J., & Bennett, G. J. (2010). Hypolocomotion, Asymmetrically Directed Behaviors (Licking, Lifting, Flinching, and Shaking) and Dynamic Weight Bearing (Gait) Changes are Not

Measures of Neuropathic Pain in Mice. *Molecular Pain*, 6(1), 34.

<https://pubmed.ncbi.nlm.nih.gov/20529328/> 10.1186/1744-8069-6-34

Murphy, N. P., Lam, H. A., & Maidment, N. T. (2001). A comparison of morphine-induced locomotor activity and mesolimbic dopamine release in C57BL6, 129Sv and DBA2 mice.

Journal of Neurochemistry, 79(3), 626-635. <https://pubmed.ncbi.nlm.nih.gov/11701766/>

10.1046/j.1471-4159.2001.00599.x

Osterweis, M., Kleinman, A., Mechanic, D., & Institute of Medicine (U.S.). Committee on Pain, Disability, and Chronic Illness Behavior. (1997). *Pain and disability : clinical, behavioral, and public policy perspectives*. University Microfilms International.

<https://www.ncbi.nlm.nih.gov/books/NBK219238/>

Pampaloni, F., Chang, B., & Stelzer, E. H. K. (2015). Light sheet-based fluorescence microscopy (LSFM) for the quantitative imaging of cells and tissues. *Cell and Tissue Research*, 360(1),

129-141. <https://pubmed.ncbi.nlm.nih.gov/25743693/> 10.1007/s00441-015-2144-5

Patel, R., & Dickenson, A. H. (2020). A study of cortical and brainstem mechanisms of diffuse noxious inhibitory controls in anaesthetised normal and neuropathic rats. *The European*

Journal of Neuroscience, 51(4), 952-962. <https://pubmed.ncbi.nlm.nih.gov/31518451/>

10.1111/ejn.14576

Perens, J., Salinas, C. G., Skytte, J. L., Roostalu, U., Dahl, A. B., Dyrby, T. B., Wichern, F.,

Barkholt, P., Vrang, N., Jelsing, J., & Hecksher-Sørensen, J. (2021). An Optimized Mouse Brain Atlas for Automated Mapping and Quantification of Neuronal Activity Using iDISCO+ and Light Sheet Fluorescence Microscopy. *Neuroinformatics (Totowa, N.J.)*, 19(3), 433-446.

<https://pubmed.ncbi.nlm.nih.gov/33063286/> 10.1007/s12021-020-09490-8

- Ramaswamy, S., & Wodehouse, T. (2021). Conditioned pain modulation—A comprehensive review. *Neurophysiologie Clinique*, 51(3), 197-208.
<https://pubmed.ncbi.nlm.nih.gov/33334645/> 10.1016/j.neucli.2020.11.002
- Reddan, M. C., & Wager, T. D. (2018). Modeling Pain Using fMRI: From Regions to Biomarkers. *Neuroscience Bulletin*, 34(1), 208-215.
<https://www.ncbi.nlm.nih.gov/pmc/articles/PMC5799128/> 10.1007/s12264-017-0150-1
- Renier, N., Adams, E. L., Kirst, C., Wu, Z., Azevedo, R., Kohl, J., Autry, A. E., Kadiri, L., Umadevi Venkataraju, K., Zhou, Y., Wang, V. X., Tang, C. Y., Olsen, O., Dulac, C., Osten, P., & Tessier-Lavigne, M. (2016). Mapping of Brain Activity by Automated Volume Analysis of Immediate Early Genes. *Cell*, 165(7), 1789-1802. <https://pubmed.ncbi.nlm.nih.gov/27238021/> 10.1016/j.cell.2016.05.007
- Renier, N., Wu, Z., Simon, D. J., Yang, J., Ariel, P., & Tessier-Lavigne, M. (2014). iDISCO: A Simple, Rapid Method to Immunolabel Large Tissue Samples for Volume Imaging. *Cell*, 159(4), 896-910. <https://pubmed.ncbi.nlm.nih.gov/25417164/> 10.1016/j.cell.2014.10.010
- Richardson, D. S., Guan, W., Matsumoto, K., Pan, C., Chung, K., Ertürk, A., Ueda, H. R., & Lichtman, J. W. (2021). Tissue clearing. *Nature Reviews Methods Primers*, 1(1)
<https://www.nature.com/articles/s43586-021-00080-9> 10.1038/s43586-021-00080-9
- Shields, S. D., Eckert, W. A., & Basbaum, A. I. (2003). Spared nerve injury model of neuropathic pain in the mouse: a behavioral and anatomic analysis. *The Journal of Pain*, 4(8), 465-470.
<https://pubmed.ncbi.nlm.nih.gov/14622667/> 10.1067/S1526-5900(03)00781-8

- Siddall, P. J., McClelland, J. M., Rutkowski, S. B., & Cousins, M. J. (2003). A longitudinal study of the prevalence and characteristics of pain in the first 5 years following spinal cord injury. *Pain*, 103(3), 249-257. <https://pubmed.ncbi.nlm.nih.gov/12791431/> 10.1016/S0304-3959(02)00452-9
- Sillitoe, R. V., & Hawkes, R. (2002). Whole-mount Immunohistochemistry: A High-throughput Screen for Patterning Defects in the Mouse Cerebellum. *Journal of Histochemistry & Cytochemistry*, 50(2), 235-244. <https://pubmed.ncbi.nlm.nih.gov/11799142/> 10.1177/002215540205000211
- Singh, A., Patel, D., Li, A., Hu, L., Zhang, Q., Liu, Y., Guo, X., Robinson, E., Martinez, E., Doan, L., Rudy, B., Chen, Z. S., & Wang, J. (2020). Mapping Cortical Integration of Sensory and Affective Pain Pathways. *Current Biology*, 30(9), 1703-1715.e5. <https://www.sciencedirect.com/science/article/pii/S0960982220302980> 10.1016/j.cub.2020.02.091
- Sørensen, A. T., Rombach, J., Gether, U., & Madsen, K. L. (2022). The Scaffold Protein PICK1 as a Target in Chronic Pain. *Cells (Basel, Switzerland)*, 11(8), 1255. <https://pubmed.ncbi.nlm.nih.gov/35455935/> 10.3390/cells11081255
- Sun, G., McCartin, M., Liu, W., Zhang, Q., Kenefati, G., Chen, Z. S., & Wang, J. (2023). Temporal pain processing in the primary somatosensory cortex and anterior cingulate cortex. *Molecular Brain*, 16(1), 3. <https://molecularbrain.biomedcentral.com/articles/10.1186/s13041-022-00991-y> 10.1186/s13041-022-00991-y
- Svendsen, O., & Lykkegaard, K. (2001). Neuronal c-Fos Immunoreactivity as a quantitative measure of stress or pain. *Acta Agriculturae Scandinavica. Section A, Animal Science*, 51(30),

131-134. <https://www.tandfonline.com/doi/abs/10.1080/090647001316923216>

10.1080/090647001316923216

Takeda, R., Watanabe, Y., Ikeda, T., Abe, H., Ebihara, K., Matsuo, H., Nonaka, H., Hashiguchi, H., Nishimori, T., & Ishida, Y. (2009). Analgesic effect of milnacipran is associated with c-Fos expression in the anterior cingulate cortex in the rat neuropathic pain model. *Neuroscience Research*, 64(4), 380-384. <https://pubmed.ncbi.nlm.nih.gov/19383518/>
10.1016/j.neures.2009.04.010

Tan, W., Yao, W., Hu, R., Lv, Y., Wan, L., Zhang, C., & Zhu, C. (2015). Alleviating Neuropathic Pain Mechanical Allodynia by Increasing Cdh1 in the Anterior Cingulate Cortex. *Molecular Pain*, 11, 56. <https://pubmed.ncbi.nlm.nih.gov/26364211/> 10.1186/s12990-015-0058-6

Tao, Y. X. (2012). AMPA receptor trafficking in inflammation-induced dorsal horn central sensitization. *Neurosci Bull*, 28(2), 111-120. <https://pubmed.ncbi.nlm.nih.gov/22466122/>

Taracha, E., Chrapusta, S. J., Lehner, M., Skórzewska, A., Maciejak, P., Szyndler, J., & Płaźnik, A. (2008). Morphine and methadone pre-exposures differently modify brain regional Fos protein expression and locomotor activity responses to morphine challenge in the rat. *Drug and Alcohol Dependence*, 97(1), 21-32. <https://pubmed.ncbi.nlm.nih.gov/18485622/>
10.1016/j.drugalcdep.2008.03.013

Vidal, J. (2016). Consistent individual differences in some behaviors in mice of the C57Bl/6J inbred strain. *Anuario De Psicología (Barcelona, Spain)*, 46(2), 83-89.
<https://www.sciencedirect.com/science/article/abs/pii/S0066512616300113>
10.1016/j.anpsic.2016.07.005

- Vowles, K. E., McEntee, M. L., Julnes, P. S., Frohe, T., Ney, J. P., & van der Goes, D. N. (2015). Rates of opioid misuse, abuse, and addiction in chronic pain: a systematic review and data synthesis. *Pain (Amsterdam)*, 156(4), 569-576. <https://pubmed.ncbi.nlm.nih.gov/25785523/> 10.1097/01.j.pain.0000460357.01998.fl
- Wang, W., Petralia, R. S., Takamiya, K., Xia, J., Li, Y., Huganir, R. L., Tao, Y., & Yaster, M. (2011). Preserved Acute Pain and Impaired Neuropathic Pain in Mice Lacking Protein Interacting with C Kinase 1. *Molecular Pain*, 7(1), 11. <https://www.ncbi.nlm.nih.gov/pmc/articles/PMC3038962/> 10.1186/1744-8069-7-11
- WHO. (2021, 55. <https://www.iasp-pain.org/advocacy/definitions-of-chronic-pain-syndromes/>. 55.
- Wu, Z., Zhang, Y., & Xiao, J. (2006). Rules of protein expression of proto-oncogene (c-Fos/c-Jun) in different brain areas and nucleus of psychological stressed mice and the regulatory effect of modified Xiaoyao Pill. *Zhongguo Zhong Xi Yi Jie He Za Zhi*, 26(11), 998-1002. <https://www.ncbi.nlm.nih.gov/pubmed/17186730>
- Yang, D., Wang, Y., Qi, T., Zhang, X., Shen, L., Ma, J., Pang, Z., Lal, N. K., McClatchy, D. B., Wang, K., Xie, Y., Polli, F., Maximov, A., Augustine, V., Cline, H. T., Yates, J. R., & Ye, L. (2023). Phosphorylation of pyruvate dehydrogenase marks the inhibition of in vivo neuronal activity. bioRxiv, <https://pubmed.ncbi.nlm.nih.gov/36993270/> 10.1101/2023.03.13.532494
- Yang, S., & Chang, M. C. (2019). Chronic Pain: Structural and Functional Changes in Brain Structures and Associated Negative Affective States. *International Journal of Molecular Sciences*, 20(13), 3130. <https://www.ncbi.nlm.nih.gov/pmc/articles/PMC6650904/> 10.3390/ijms20133130

Yau, C. N., Lai, H. M., Lee, K., Kwok, A. J., Huang, J., & Ko, H. (2023). Principles of deep immunohistochemistry for 3D histology. *Cell Reports Methods*, 3(5), 100458.

<https://www.sciencedirect.com/science/article/pii/S2667237523000772>

10.1016/j.crmeth.2023.100458

Appendices

Appendix 1: Protocol for tissue clearing and immunolabeling.

Protocol for tissue clearing and immunolabeling of the naive and SNI mice.

Chemicals

Chemical	Abbreviation	Contents + concentration	Supplier	LOT/CAS/ Cat no.
Dichloromethane	DCM	100% or 2:1 DCM/methanol (40/20 mL)	Sigma-aldrich	34977
Ethyl cinnamate	ECi	98% stabilized	Sigma-aldrich	800238
Methanol	MeOH	100% or 80, 60, 40, 20% mixed with PBS or MiliQ water	VWR chemicals	85802.290
Dimethyl sulfoxide	DMSO	500 mL: 100 mL DMSO	Sigma Aldrich	276855
Triton x-100		0,2% in PBS	Sigma Aldrich	11332481001
Glycine		General blocking solution: 11,5 g	Sigma Aldrich	410225
Heparin		1 g	Sigma-Aldrich	H3149
Sodium azide	NaN ₃	5%	Sigma-Aldrich	71289
PBS Solution	PBS tablet	5 g PBS tablet in 500 mL mQ water: 70 mM NaCl, 5 mM phosphate buffer, 1,5 mM KCL + 0,02% sodium azide. pH 7,45	GiboTm	11514526
Gelatin from porcine skin		0,2%	Sigma-Aldrich	G2500
Tween 20		2 mL in washing buffer	Sigma-Aldrich	P1379
Primary antibody		1:3000	Cell signaling	22505

Secondary antibody		1:1000	Jackson immune research labs	NC0245384
Isoflurane		4% in PBS	Piramal	055226
Ammonium		5% in miliQ water	Fischer Scientific	64016
Quadrol		25% in MQ water	Sigma Aldrich	122262
Paraformaldehyde solution	PFA	4% buffered	Sigma Aldrich	100496
PBS with triton x-100 and heparin	PTxH	1 L: 2 mL triton, 1 L PBS, 1 mL 10mg/mL Heparin + 0.02% azide (NaN ₃)	Mixed in the laboratory	
PBS with tween 20 and heparin	PTwH	1 L: 2 mL tween 20, 1 L PBS, 1 mL of 10mg/mL Heparin + 0.02% azide (NaN ₃)	Mixed in the laboratory	

Procedure for the use of c-Fos antibody

iDISCO+

Study nr: 2023061123
No. of animals: 24 No. of
groups: 3
8 brains/group
Primary antibody: anti-c-FOS
(9F6) Rabbit Secondary
antibody: anti-Rabbit 647



	Treatment	IN	Duration	Notes
	Perfusion + dissection	6.11.23		
	4% PFA (post-fixation)	06.11.2023	O/N at 4°C	
	Wash PBS (w. 0.02% azide)	7+8 nov	a few washes over 1h RT	RT = room temp
	25% Quadrol in water	13.11.23	2-3 days at 37°C	make Quadrol solution fresh, be sure that the samples are placed on their side for optimal solution agitation
	5% ammonium in water	16.11.2023	1 day at 37°C	does not need to be made fresh if there is enough in stock. 108.33 mL 30% ammonium til 541.67 mL miliQ
	20% MeOH in water	17.nov	1 hour at RT	Liedown on shaker
	40% MeOH in water	17.nov	1 hour at RT	Liedown on shaker
	60% MeOH in water	17.nov	1 hour at RT	Liedown on shaker
	80% MeOH in water	17.nov	1 hour at RT	Liedown on shaker
	100% MeOH in water	17.nov	1 hour at RT	Liedown on shaker
	100% MeOH in water	17.nov	1 hour at RT	Liedown on shaker
	2:1 DCM/MeOH	17.nov	O/N at RT	
	100% MeOH	18.nov	2-3 washes at RT	
	5% H2O2 / MeOH (bleaching)	18.nov	O/N at 4°C	make sure the solution and the sample are both cold before changing
	80% MeOH in water	19.nov	1 hour at RT	Liedown on shaker
	60% MeOH in water	19.nov	1 hour at RT	Liedown on shaker
	40% MeOH in water	19.nov	1 hour at RT	Liedown on shaker
	20% MeOH in water	19.nov	1 hour at RT	Liedown on shaker
	PBS	19.nov	1 hour at RT	Liedown on shaker, store in PBS at 4C for 7 days samples
	General Permeabilization Solution	20.nov	O/N at 37°C	
	General Blocking Solution	21.nov	O/N at 37°C	
	Primary Antibody (1:3000)	22.nov	14 days at 37°C	primary antibody: anti-c-FOS (9F6)
	PTwH	02.dec	2 days, change the solution 4/5X	
	Secondary Antibody (1:1000)	04.dec	8 days at 37°C	anti-Rabbit 647 from Jackson immuno research, in freezer (Gith's box)
	PTwH	12.dec	Do 3 washes	
	2% PFA postfix at rt	12.dec	1 hour at RT	
	PTwH	12.dec	Do 3 washes change solution 3/4X on Fri	Step 30-32 (Washes and PFA) do over 2 days at least
	20% MeOH in water	13.12.2023	1 hour at RT	Liedown on shaker
	40% MeOH in water	13.12.2023	1 hour at RT	Liedown on shaker
	60% MeOH in water	13.12.2023	1 hour at RT	Liedown on shaker
	80% MeOH in water	13.12.2023	1 hour at RT	Liedown on shaker
	100% MeOH	13.12.2023	1 hour at RT	Liedown on shaker
	100% MeOH	13.12.2023	1 hour at RT	Liedown on shaker
	66% DCM / 33% MeOH	13.12.2023	O/N at RT	Do not lie down
	100% DCM	14.12.2023	30 mins at RT	Do not lie down
	100% DCM	14.12.2023	30 mins at RT	Do not lie down
	ECi	14.12.2023	indefinitely	Fill the tube
	Imaging on Zeiss Light Sheet 7	4+5+7.12		
	General Permeabilization Solution (500 mL)			Other notes: Tissue can turn opaque over time when in contact with air, reduce air by filling the tubes to the tippy top when storing them in the final clearing solution (ECi)
	400 mL PTxH			
	11.5 g of Glycine			
	100 mL of DMSO			

General Blocking Solution (500 mL)
500 mL PTxH
1 g gelatin (0.2%)

PTxH (1 L)
2 mL triton
1 L PBS from tablet
1 mL of 10mg/mL Heparin
2 mL of 5% azide (NaN3) (0.02% conc.)

PTwH (1 L)
2 mL tween 20
1 L PBS
1 mL of 10mg/mL Heparin
2 mL of 5% azide (NaN3) (0.02% conc.)

PBS (1 L)
dissolve 2 tablets of "PBS" in 1 L water
2 mL of 5% azide (NaN3) (0.02% conc.)

Procedure for the use of pPDH antibody

iDISCO+

Study nr: xx
 animals: 6
 groups,
 3 brains/group
 No. of groups: 2
 Primary antibody: Phospho-
 Pyruvate Dehydrogenase α 1
 (Ser293) Antibody #31866
 Secondary antibody: anti-Rabbit
 647



Treatment	IN	Duration	Notes
Perfusion + dissection	18.10.2023		
4% PFA (post-fixation)	18.10.2023	O/N at 4°C	
Wash PBS (w. 0.02% azide)	19.10.2023	a few washes over 1h RT	RT = room temp
25% Quadrol in water	29.10.2023	2-3 days at 37°C	make Quadrol solution fresh, be sure that the samples are placed on their side for optimal solution agitation
5% ammonium in water	01.11.2023	1 day at 37°C	does not need to be made fresh if there is enough in stock. 108.33 mL 30% ammonium til 541.67 mL milliQ
20% MeOH in water	02.nov	1 hour at RT	Lie down on shaker
40% MeOH in water	02.nov	1 hour at RT	Lie down on shaker
60% MeOH in water	02.nov	1 hour at RT	Lie down on shaker
80% MeOH in water	02.nov	1 hour at RT	Lie down on shaker
100% MeOH in water	02.nov	1 hour at RT	Lie down on shaker
100% MeOH in water	02.nov	1 hour at RT	Lie down on shaker
2:1 DCM/MeOH	02.nov	O/N at RT	
100% MeOH	03.nov	2-3 washes at RT	
5% H2O2 / MeOH (bleaching)	03.nov	O/N at 4°C	make sure the solution and the sample are both cold before changing
80% MeOH in water	04.nov	1 hour at RT	Lie down on shaker
60% MeOH in water	04.nov	1 hour at RT	Lie down on shaker
40% MeOH in water	04.nov	1 hour at RT	Lie down on shaker
20% MeOH in water	04.nov	1 hour at RT	Lie down on shaker
PBS	04.nov	1 hour at RT	Lie down on shaker, store in PBS at 4C for 7 days samples
General Permeabilization Solution	06-11-2023 (1,3,4,6), 13/11 (2,5)	O/N at 37°C	
General Blocking Solution	07-11-2023 (1,3,4,6), 14/11-2023 (2,5)	O/N at 37°C	
Primary Antibody (1:500)	08-11-2023 (1,4)	14 days at 37°C	1 and 4, Phospho-Pyruvate Dehydrogenase α 1 (Ser293) Antibody #31866
Primary Antibody (1:250)	15/11-2023 (2,5)	7 days at 37°C	2 and 5, Phospho-Pyruvate Dehydrogenase α 1 (Ser293) Antibody #31866
Primary Antibody (1:250)	08-11-2023 (3,6)	14 days at 37°C	3 and 6, Phospho-Pyruvate Dehydrogenase α 1 (Ser293) Antibody #31866
PTwH	22.nov	2 days, change the solution 4/5X	
Secondary Antibody (1:1000)	25.nov	8 days at 37°C	anti-Rabbit 647 from Jackson immuno research, in freezer (Gith's box)
PTwH	04.dec	Do 3 washes	
2% PFA postfix at rt	04.dec	1 hour at RT	
PTwH	04.dec	Do 3 washes	Step 30-32 (Washes and PFA) do over 2 days at least
20% MeOH in water	06.12.2023	1 hour at RT	Lie down on shaker
40% MeOH in water	06.12.2023	1 hour at RT	Lie down on shaker
60% MeOH in water	06.12.2023	1 hour at RT	Lie down on shaker
80% MeOH in water	06.12.2023	1 hour at RT	Lie down on shaker
100% MeOH	06.12.2023	1 hour at RT	Lie down on shaker
100% MeOH	06.12.2023	1 hour at RT	Lie down on shaker
66% DCM / 33% MeOH	06.12.2023	O/N at RT	Do not lie down
100% DCM	07.12.2023	30 mins at RT	Do not lie down
100% DCM	07.12.2023	30 mins at RT	Do not lie down
ECi	07.12.2023	indefinitely	Fill the tube
Imaging on Zeiss Light Sheet 7	4+5+7.12		
General Permeabilization Solution (500 mL)			Other notes: Tissue can turn opaque over time when in contact with air, reduce air by filling the tubes to the tippy top when storing them in the final clearing solution (ECi)

400 mL PTxH
 11.5 g of Glycine
 100 mL of DMSO

General Blocking Solution (500 mL)
 500 mL PTxH
 1 g gelatin (0.2%)

PTxH (1 L)
 2 mL triton
 1 L PBS from tablet
 1 mL of 10mg/mL Heparin
 2 mL of 5% azide (NaN3) (0.02% conc.)

PTwH (1 L)
 2 mL tween 20
 1 L PBS
 1 mL of 10mg/mL Heparin
 2 mL of 5% azide (NaN3) (0.02% conc.)

PBS (1 L)
 dissolve 2 tablets of "PBS" in 1 L water
 2 mL of 5% azide (NaN3) (0.02% conc.)

Appendix 2: total c-Fos positive cells detected in the SNI mice for each brain in the three different groups: PBS, morphine, mPD5

Table 3. Whole brain cell counts for the SNI treated mice. Group A was treated with PBS. Group B was treated with 10 mg/kg Morphine. Group C was treated with 10 μ mol/kg mPD5.

PBS		Morphine		mPD5	
IDs	Cell counts	IDs	Cell counts	IDs	Cell counts
9	43880	1	211415	17	21082
11	30323	3	80583	19	26707
13	32813	5	95392	21	26951
15	42217	7	97996	23	34107
25	29289	41	91090	33	36726
27	37752	43	120520	35	28370
29	16729	45	62926	37	32390
31	25603	47	98638	39	33556
Average	32325	Average	107320	Average	29986

Appendix 3: total c-Fos positive cells detected in the naive mice for each brain in the three different groups: PBS, morphine, mPD5

Table 4. Whole brain cell counts for the naive treated mice. Group A was treated with PBS. Group B was treated with 10 mg/kg Morphine. Group C was treated with 10 μ mol/kg mPD5. In group C there is missing data on one mouse due to destroyed brain tissue.

PBS		Morphine		mPD5	
IDs	Cell counts	IDs	Cell counts	IDs	Cell counts
9	29182	1	105892	19	28410
11	28255	3	128375	21	29959
13	25435	5	87916	23	30440
15	45354	7	139866	41	43469
33	14377	49	138078	43	34084
35	30537	51	155688	45	28943
37	25939	53	117729	47	33922
39	25376	55	136060		
Average	28057	Average	126200	Average	32746

Appendix 4: Data from the naive morphine-treated and PBS-treated cohort

Table 5. The first column is the name of the region and in parentheses the abbreviation used for the region in the volcano plot and in the text. The second and third columns are lists of the average cell counts in the given region across the morphine treated group (second column) and the PBS treated group (third column) with the standard deviation (STD) in parentheses. The fourth column is the fold-change calculated as: $FC = \frac{\text{average cell count for morphine}}{\text{average cell count for PBS}}$.

Data from morphine vs PBS			
Region (abbreviation)	Morphine average cell count (STD)	PBS average cell count (STD)	Fold-change
Ventral Tegmental area (VTA)	199 (89)	32 (18)	6.2
Prelimbic area, layer 2/3 (PL2/3)	102.38 (45)	10.88 (7)	9.4
Secondary motor area, layer 5 (MOs5)	4180.88 (1512)	219.12 (120)	19
Secondary motor area, layer 6a (MOs6a)	2596.75 (577)	184.75 (88)	14
Primary motor area, layer 6a (MOp6a)	3299 (724)	262.38 (103)	12